Department of Physics
University of Helsinki
Finland

Traceability for nanometre scale measurements

Atomic force microscopes in dimensional nanometrology

Virpi Korpelainen

ACADEMIC DISSERTATION

To be presented, with the permission of the Faculty of Science of the University of Helsinki, for public examination in Aud XII, University main building, on 26 November 2014, at 12 noon.

Helsinki 2014

ISBN 978-952-6682-20-4 (pbk.)
ISBN 978-952-6682-21-1 (PDF)

Helsinki 2014

Abstract

Reliability of measurement is a crucial element of both research and industry. Metrological traceability to the SI unit metre guarantees commensurate units, also at nanometre range. In this thesis, a traceability chain is established for nanometre scale measurements. Measurement instruments and methods were developed for accurate measurements, calibration of instruments and transfer standards, and uncertainty estimations. A metrological atomic force microscope (MAFM) was developed and characterized. The MAFM can be used in the calibration of transfer standards and in accurate AFM measurements. Calibration methods for commercial AFMs were developed. A laser diffractometer was also developed for accurate calibration of 1-D and 2-D gratings with a standard uncertainty of several tens of picometres.

Laser interferometric position measurement with a calibrated vacuum wavelength is directly traceable to the realization of the metre if measuring full interferometer fringes, but there is small nonlinearity in sub-fringe measurements. Therefore, in sub-nanometre measurements the nonlinearity of the interferometer needs to be corrected. A method for this correction was developed.

Laser diffraction measurement is a very accurate method for characterization of grating pitch. One of the main uncertainty sources is the uncertainty of the measured diffraction angle. Therefore, a method for calibration of the rotary table of the laser diffraction setup was developed. The method can be used also in the realization of angle scale.

Methods for transfer standard calibration were developed for both pitch and step height calibration by MAFM.

An acoustic method was developed for compensation of the refractive index of air in interferometric measurements. Sub-nanometre uncertainty can be reached with this method.

Characterization of instruments, validation of methods and uncertainty estimations are a crucial part of traceability. Therefore, uncertainty estimates based on the characterization of the instruments are given for all measurements in this thesis.

Comparisons between laboratories are the best way to ensure commensurate measurements. International comparison results between national metrology institutes for pitch and step height transfer standards are listed.

Acknowledgements

The research work for this thesis was carried out at the Centre for Metrology and Accreditation (Mittatekniikan keskus, MIKES) in 2002-2013.

I would like to thank my supervisor, Dr Antti Lassila, for introducing me to length metrology, and for all his support and motivation during the long years of research. I am also grateful Professor Timo Hirvi and Dr Heikki Isotalo for the opportunity to carry out the work for this thesis at MIKES.

I would like to thank all my colleagues at MIKES, especially MSc Jeremias Seppä, Mr Asko Rantanen, PhD Hannu Husu and MSc Aarni Iho, and the whole length group. It has been a pleasure working with you.

Many thanks to PhD Mikko Merimaa for the discussions and comments on the thesis.

Thanks also to PhD Kaj Nyholm for his valuable comments.

I am grateful to Mr Leonid Mihaljov and AcWaCo Ltd for their kind co-operation.

I would like to thank all my international colleagues for their co-operation and valuable input throughout the years.

I am also thankful to the University of Helsinki, Department of Physics, and Professor Juhani Keinonen for the inspiring atmosphere during my studies and initial years in the academic world, and to Professor Jyrki Räisänen for his support at the very end of the work.

Many thanks to the preliminary examiners Professor Janne Ruokolainen and Professor Markus Ahlskog for their effort.

Thanks to Adelaide Lönnberg for revising the English language of the thesis.

I would like to acknowledge the Academy of Finland for the financial support, and NGS-NANO for their support.

Finally, I would thank my family, Ilkka and Lassi, for their encouragement and support.

Contents

Abstract 3

Acknowledgements 4

List of original publications 7

Author's contribution 8

Scientific contribution 9

Abbreviations 10

List of symbols 12

1 Introduction 14

2 International system of units (SI) 16

2.1 Traceability, measurement uncertainty and calibration 16

2.2 The Metre 17

2.3 Derived units: the radian 18

3 Laser interferometry 19

3.1 Refractive index of air 20

3.1.1 Acoustic method for determination of the refractive index of air 20

3.1.1.1 Equations 21

3.1.1.2 Setup 21

3.1.1.3 Results 23

3.2 Interferometer nonlinearity 25

3.2.1 Method 26

3.2.2 Setup and measurements 26

3.2.3 Results 26

4 Scanning probe microscopy 30

4.1 Traceability of SPM measurements 32

4.2 Calibration principles of SPMs 34
4.3 MIKES metrological AFM 37
4.3.1 Setup 38
4.3.2 Measurement principle 38
4.3.3 Traceability and uncertainty of the IT-MAFM 39
4.4 Calibration of transfer standards 41
4.5 Calibration of an AFM 43
4.6 Results 45
5 Laser diffractometer 47
5.1 Principle of laser diffraction 47
5.2 Measurement setup 48
5.3 Traceability and uncertainty of the diffractometer measurement 49
5.3.1 Traceability of the angle scale 50
5.4 Results 51
6 Discussion 53
7 Conclusions 55
References 56

List of original publications

This thesis is based on the following publications:

I V. Korpelainen, A. Iho, J. Seppä and A. Lassila, "High accuracy laser diffractometer: Angle-scale traceability by error separation method with a grating" *Measurement Science and Technology*, **20** 084020 (8pp), 2009

II V. Korpelainen, J. Seppä and A. Lassila, "Design and characterization of MIKES metrological atomic force microscope" *Precision Engineering* **34** 2, 735-744, 2010

III V. Korpelainen, J. Seppä and A. Lassila, "Measurement strategies and uncertainty estimations for pitch and step height calibrations by metrological atomic force microscope" *Journal of Micro/Nanolithography, MEMS and MOEMS*, **11**(1), 011002, 2012

IV V. Korpelainen and A. Lassila, "Calibration of a commercial AFM: traceability for a coordinate system" *Measurement Science and Technology*, **18**, 395-403, 2007

V V. Korpelainen and A. Lassila, "An acoustic method for determination of the effective temperature and refractive index of air in accurate length interferometry" *Optical engineering* **43**, 2400-2409, 2004.

The publications are referred to in the text by their Roman numerals.

Author's contribution

All the publications included in this thesis are results of teamwork.

For publication I, the author designed, carried out and analysed preliminary measurements with a temporary setup and part of the published results, and prepared the manuscript.

For publication II, the author was active in the design and construction of the instrument, designed, carried out and analysed most of the measurements, calculated the uncertainties, and prepared the manuscript.

For publication III, the author carried out most of the measurements, analysed the results, calculated the uncertainties and prepared the manuscript.

For publication IV, the author designed and carried out the measurements, analysed the results, calculated uncertainties, and prepared the manuscript.

For publication V, the author designed the measurement setup, designed and carried out the measurements, analysed the results, fitted the equations, calculated uncertainties, and prepared the manuscript.

Scientific contribution

This thesis contains the following new scientific results:

I-IV The scientific work in these four publications together completes the traceability chain for nanometre scale measurements in Finland, and enables calibration services. The results will improve the accuracy of nanometre scale measurements especially in Finland and Northern Europe. The instruments and methods developed in the papers are a basis for further studies in nanometrology at MIKES.

I Design of a fully automated high accuracy laser diffractometer with novel use of a CCD camera in measurement and alignment of the system.
A new realization method for the SI unit radian and calibration method for rotary tables.
The results will improve the accuracy of pitch calibration and angle measurements.

II Design of an interferometrically traceable metrological atomic force microscope.
Characterization of the instrument and uncertainty estimates.
A new correction method for laser interferometer nonlinearity.
The results will improve the accuracy of nanometre scale measurements.

III Uncertainty estimates for calibration of pitch and step height based on uncertainty of the coordinate system of the AFM.
New calibration strategies, which reduce measurement time, noise and uncertainty of the measurements, for pitch and step height calibrations.
The results will improve the accuracy of transfer standard calibrations and reduce measurement time.

IV Calibration and characterization methods for an AFM and uncertainty estimates for the coordinate system.
The uncertainty budget can be used as an example when estimating uncertainties of other microscopes.
The results will improve the accuracy of nanometre scale measurement.

V Development and validation of a new acoustic method for measurement of the refractive index of air. The results will improve the accuracy of interferometric measurements.

Abbreviations

A*STAR	National metrology institute of Taiwan
AFM	Atomic force microscope/microscopy
AIST	Advanced industrial science and technology, Japan
APT	Acoustic piezo transduser
BIPM	Bureau International des Poids et Measures
CC	Cube corner
CCD	Charged couple detector
CCL	Consultative committee in length
CIPM	Comité international des poids et mesures, International Committee for Weights and Measures
CGPM	Conférence Générale des Poids et Mesures, General Conference on Weights and Measures
CMC	Calibration and Measurement Capabilities
CMI	Český metrologický institute, Czech Republic
CMS/ITRI	The Center for Measurement Standards of Industrial Technology Research Institute, Taiwan
DAQ	Data acquisition card
DFM	Dansk Fundamental Metrologi
EFM	Electrostatic force microscope/microscopy
EMRP	European metrology research program
GUM	Guide to the Expression of Uncertainty in Measurement
INRIM	Istituto Nazionale di Ricerca Metrologica, Italy
IT-MAFM	Interferometrically traceable metrological atomic force microscope
JQA	Japan Quality Assurance Organization
KRISS	Korea research institute of standards and science
LNE	Laboratoire National de Métrologie et d'Essais, France
MAFM	Metrological atomic force microscope
METAS	Bundesamt für Metrologie, Federal Office of Metrology, Switzerland
MFM	Magnetic force microscope/microscopy
MIKES	Mittatekniikan keskus, Centre for Metrology and Accreditation
MRA	Mutual recognition arrangement
NIM	National Institute of Metrology, China
NIST	National Institute of Standards and Technology
NMI	National Metrology Institute
NMIA	National Measurement Institute, Australia
NMIJ	National Metrology Institute of Japan
NMi-VSL	Netherlands' National Metrology Institute - Van Swinden Laboratory
NPL	National Physical Laboratory, UK
NRC	National Research Council, Canada
PBS	Polarizing beam splitter
PSD	Position sensitive detector
PTB	Physikalisch-Technische Bundesanstalt, Germany

SFM	Scanning force microscope/microscopy
SI	Système International d'Unités, International system of units
SPM	Scanning force microscope/microscopy
STM	Scanning tunnelling microscope/microscopy
TOF	Time of flight
VNIIM	D.I. Mendeleev All-Russian Institute for Metrology
WGDM	Working group on dimensional measurements

List of symbols

α	angular position
α_t	coefficient for thermal expansion
$\delta\alpha$	angle error
$\delta\varphi_{nonlin,i}$	correction for interferometer nonlinearity in *i* direction
$\delta h_{local\ variations}$	error caused by local step height variations
δl_{Abbe}	Abbe error
$\delta p_{local\ variations}$	error caused by local pitch variations
δx, δy, δz	Abbe offset in X, Y and Z directions
δx_{drift}, δy_{drift}, δz_{drift}	drift in X, Y and Z directions
$\delta x_{deadpath}$,$\delta y_{deadpath}$, $\delta z_{deadpath}$	dead path error in X, Y and Z directions
δx_{flat}, δy_{flat}	flatness error in X and Y mirror
δz_{oop}	out-of-plane error in Z direction
γ_{ij}	angle between *i* and *j* axes
γ_0, γ_{90}	measured angles between horizontal and vertical directions in different sample orientations
λ	wavelength
λ_0	vacuum wavelength
γ_s	angles between horizontal and vertical lines of 2-D grating
ξ	angle between measurement axis and measurement line
θ_m	diffraction angle for *m*th diffraction order
τ	grating tilt
$\Delta\alpha$, $\Delta\alpha_{pitch,\ yaw,\ roll,i}$	(pitch. yaw or roll) angle change in full range of *i* axis
Δx	resolution in *x* direction
Ω	grating roll
$\Delta t_{20℃}$	temperature deviation from 20℃
ΔX, ΔY, ΔZ	full X, Y and Z ranges
L	length
$a_{i,j}$	component of matrix **A**
$c_{i,j}$	components od matrix **C**
k, k_i	number of interferometer fringes (in *i* direction), or number of measured pitches
n, n_i	refractive index (of air) along *i* axis
C, C_x, C_y, C_z	scale correction for X, Y and Z axis
H	nominal step height
L, L_k	measured length
P	nominal pitch
S_{rate}	scan rate
S_{range}	scan range
W_m	normalized weight for *m*th diffraction order
W	width of a step
c_0	speed of light
f	frequency

h, h_i	step height
m	diffraction order
p	pitch
p_{cal}	calibrated pitch
p_m	pitch calculated from *m*th diffraction order
u_c	standard uncertainty
w_m	weight for *m*th diffraction order
x_m, y_m, z_m	measured X, Y and Z coordinates
$\overline{z_i}$	average over area *i*
$\mathbf{r}$	coordinates [x, y, z]
$\mathbf{C}$	correction matrix for non-orthogonal axes
$\mathbf{A}$	correction matrix for Abbe error
$\mathbf{m}$	measured coordinates [x_m, y_m, z_m]
$\mathbf{D}$	correction vector including drift, dead path, flatness or out-of-plane

1 Introduction

Scientific research and the commercialization of inventions are not possible without reliable measurements. One of the fundamental principles of scientific research is that measurements must be comparable even if performed with different instruments by different people at different times. This necessitates the use of commensurate units.

> Metrology is the science of measurement and its application. Metrology includes all theoretical and practical aspects of measurement, whatever the measurement uncertainty and field of application. [1]

Metrology has a long tradition. Reliable measurements have always been essential for fair trade and industry; the Industrial Revolution and advent of mass production could not have happened without them. Emerging fields of research and industry place ever-newer demands on measurements also today. One such field is nanotechnology, a fast growing field that was long at basic research level, but that in recent years has exploded onto the scene of practical applications and commercial products. Imaging techniques for nano-objects are an important part of this development, among them various types of high-resolution microscope. However, high resolution does not necessarily equate to high accuracy; new reliable measurement methods are needed for nanotechnology, and nanometrology is the answer. Nanometrology is an enabling technology. Dimensional nanometrology is defined as follows:

> Dimensional nanometrology is the science and practice of measurement of the dimensions of objects or object features, separations or displacements in the range from 1 nm to 1000 nm. [2]

Metrological traceability and calibration are needed in all measurements, but old calibration methods are not suitable at nanometre scale. The roadmap of “Dimensional metrology for micro- and nanotechnologies” lists four core applications/technologies: nanoparticles, functionalized surfaces, semiconductor & nanoelectronics, and nanobiotechnology [3]. Reliable measurements are hugely important in regards to safety and health.

In this thesis, traceable measurements and calibration methods are developed for accurate measurements at nanometre scale. The research carried out here is a fundamental stepping stone to the research listed in the roadmap. To this end we have developed an interferometrically traceable metrological atomic force microscope (IT-MAFM) [II]. Uncertainty estimates for pitch and step height calibration with the metrological AFM were calculated and new measurement strategies introduced [III]. A traceable laser diffractometer was developed for calibration of grating pitch [I]. These two independent methods were compared to each other and to other MAFMs in an international comparison [4]. Calibration methods for a commercial AFM were developed and the resulting uncertainty was calculated [IV]. To reduce the uncertainty of an interferometric

displacement measurement, a novel ultrasound method was developed for measuring the refractive index of air within an interferometer beam path [V].

Section 2 explains the international system of units (SI) and some basic concepts of metrology, with an emphasis on length metrology.

Section 3 focuses on laser interferometry. The most accurate length measurements are done using this method. In short-range measurements, periodical nonlinearity of the interferometer is a significant error component. Therefore, in this thesis a method for measurement and compensation of the error was developed [II]. In longer scale measurement, for the most accurate measurements or outside ideal laboratory conditions it is a challenge to measure the refractive index of air accurately. We have developed a new method to compensate for the refractive index of air [V].

Sections 4 and 5 concern the traceability and calibration of scanning probe microscopes (SPMs), and the calibration of step height and pitch standards for use in the calibration. A metrological atomic force microscope (MAFM) [II] and laser diffractometer [I] were developed for calibration of calibration standards. Calibration methods for transfer standards [III] and an atomic force microscope (AFM) were also developed [IV].

Nanometrology has been a focal point at many National Metrology Institutes (NMIs) for the past 15 years. More than 20 metrological AFMs have either been developed or are in progress (see chapter 4 and Table 1), and more than 10 laser diffractometers have been developed (Table 2). Several international comparisons in nanometrology have been organized at nanometre scale for grating pitch (CCL-Nano4 [5] CCL-Nano5 [6] and Euramet 925 [4]) and step height [4, 7, 8]. Measurement methods and instruments for nanometre scale measurements have been or are being developed as part of the European Metrology Research Program (EMRP) in projects such as MetNEMS [9, 10], MechProNO [11], Scattero [12], SubNano [13], and CRYSTAL [14].

2 International system of units (SI)

The origin of the international system of units (Système International d'Unités, SI) dates back to the French revolution. The French National Assembly introduced the decimal metric system on April 7, 1795 with the law "On weights and measures". The defined units were the metre and the kilogram. The revolutionary idea was that the measurement units should be based on constants of nature and thus available “for all men and all time”. The archive metre was defined as being equal to the ten millionth part of one quarter of the terrestrial meridian and the kilogram was defined as the mass of a cubic decimetre of water. The first standards of the metre and the kilogram, against which all future copies were to be compared, were deposited in the Archives of the French Republic in 1799.

A step towards a global unit system was the signing of the Metre Convention by 17 countries in 1875. As of 2014 there are 55 member states and 33 associate states or economies. Finland became a member state 1923. The name International System of Units with the abbreviation SI has been used since 1960.

The metrology system has arisen from the challenges posed by the measurement requirements of science and industry. Over time the number of base units has risen from three to seven; in 1875 the metre, kilogram and second were approved as base units, added to in 1954 by the ampere, the kelvin and the candela, and in 1971 by the mole. Greater accuracy requirements and advancing scientific development have necessitated several changes in the definitions of units. The definition of the metre has changed twice (in 1960 and 1983) and that of the second once (in 1967/68). The next modification to the SI system will probably be in 2015. It is proposed to redefine the kilogram in terms of the Planck constant, the ampere in terms of the electron charge, the kelvin in terms of the Boltzmann constant, and the mole in terms of the Avogadro constant. Following these redefinitions the original idea of the SI will have finally been reached — a unit system based on the constants of nature.

2.1 Traceability, measurement uncertainty and calibration

Metrological traceability is one of the leading principles in this thesis and is defined as:

> The property of a measurement result whereby the result can be related to a reference through a documented unbroken chain of calibrations, each contributing to the measurement uncertainty [1].

The traceability chain is defined as:

> A sequence of measurement standards and calibrations that is used to relate a measurement result to a reference [1].

Uncertainty of measurement is closely related to traceability and is defined as:

> A non-negative parameter characterizing the dispersion of the quantity values being attributed to a measurand, based on the information used [1].

Guidelines given in the Guide to the Expression of Uncertainty in Measurement (GUM) [15] are generally used in uncertainty estimations. The GUM is used in the analysis of uncertainties in this thesis.

International trade and the elimination of trade barriers require the adoption of commonly accepted measurements. The Mutual Recognition Arrangement (Comité International des Poids et Mesures (CIPM) MRA) has been signed by 84 NMIs or international organizations and covers 137 institutes. Under the MRA, all participating institutes recognize the validity of each other's calibration and measurement certificates for the quantities, ranges and measurement uncertainties specified in Calibration and Measurement Capabilities of NMIs (CMCs).

Without traceability, measurement results are not comparable with other results, the measurements cannot be repeated, and measurement instruments cannot be replaced with other instruments. In trade, the need for commensurate units and traceability is evident. Buyer and seller must use the same units in their measurements. In scientific research, all published results have to be traceable to the SI, or any further research referring to the publication will lack traceability too.

In practice, traceability is usually attained by careful calibration of measurement instruments using calibrated transfer standards. Calibration is:

> An operation that, under specified conditions, in a first step, establishes a relation between the quantity values with measurement uncertainties provided by measurement standards and corresponding indications with associated measurement uncertainties and, in a second step, uses this information to establish a relation for obtaining a measurement result from an indication [1].

New measurement techniques have been developed for nanotechnology research and manufacture. Good resolution of instruments may give an illusion of good accuracy, but high resolution does not necessarily translate to high accuracy. Comparability of measurements is reached only if the measurements are traceable to the realizations of the SI units. In this thesis, calibration methods have been developed for nanotechnology.

2.2 The Metre

In this thesis, the developed methods and instruments are traceable to the metre and radian. Therefore, the definitions and realizations of these units are discussed in detail.

The first definition of the SI unit metre from 1889 was the international prototype of platinum-iridium. Over the years, measurement methods improved and accuracy requirements grew. The realization of the metre no longer met the accuracy requirements of research and industry, and the metre was redefined in 1960. The new definition of the

metre was based on the wavelength of krypton 86 radiation. In 1983 at the 17th CGPM (1983, Resolution 1) the metre was given its current definition:

> The metre is the length of the path travelled by light in vacuum during a time interval of 1/299 792 458 of a second.

The definition means that speed of light in vacuum is defined as a natural constant c_0 = 299 792 458 m/s.

The definition of the metre links it to the definition and realization of the second. The second is defined as the duration of

> 9 192 631 770 periods of the radiation corresponding to the transition between the two hyperfine levels of the ground state of the caesium 133 atom.

Practical realization of the metre is done using stabilized lasers with measured frequency f and thus vacuum wavelength λ_0:

$$\lambda_0 = \frac{c_0}{f}. \qquad (1)$$

2.3 Derived units: the radian

In addition to the SI base units there are several derived units. One of them is the unit of plane angle, the radian, which is defined as:

> A plane angle between two radii of a circle which cut off on the circumference an arc equal in length to the radius.

Due to the definition of the radian, one full circle, i.e. 2π rad or 360° angle, can be taken as an error-free angle standard. Division of a circle then realizes the unit radian. The classical error separation method for angle calibration is based on this concept [16, 17]. A basic idea in error separation is that errors of the measurement instrument and the sample can be separated by repeated measurements in different sample orientations.

3 Laser interferometry

Laser interferometry is a tool for measuring physical dimensions using the wavelength of a laser light. A simplified idea in laser interferometry is to use laser wavelength (λ) as a ruler and to count how many (k) wavelengths (λ) are on the measured length l

(2) $$l = k\lambda \, .$$

The principle of a simple Michelson type laser interferometer is shown in Figure 1. The laser beam is split into measurement and reference arms by a beam splitter. Both beams are reflected back from mirrors or retroreflectors and combined beyond the beam splitter. Interference of the beams is seen in the detector. Depending on the phase difference between the measurement and reference beam, a constructive or destructive interference is seen in the detector. When the measurement mirror moves, constructive and destructive interference are seen in turn, and number of interferometer fringe distances can be counted. Because the beam travels back and forth, the distance between two interferometer fringes equals a distance of $\lambda/2$ in a single pass interferometer. In double pass interferometers, the beam reflects twice from the measurement and reference mirrors and thus the distance between two interferometer fringes equals a distance of $\lambda/4$. Sub-fringe accuracy can be reached using phase information in addition to counting full fringes.

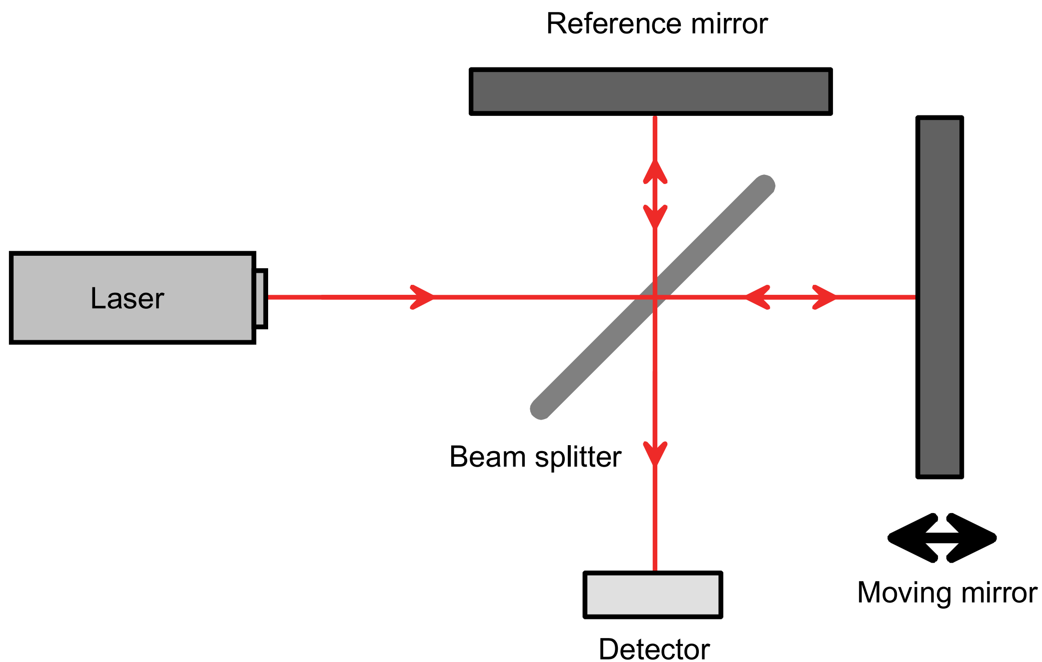

Figure 1 *Principle of a Michelson type interferometer.*

The interferometers used in the studies of this thesis are heterodyne interferometers, where the measurement beam and reference beam have slightly different frequencies and orthogonal polarizations. The laser beam is split to the measurement and reference arms using a polarizing beam splitter. To direct both beams to the detector, quarter wave ($\lambda/4$) plates are used to change the vertical polarization into horizontal mode and vice versa. The movement is detected as a phase change between the reference and measurement arms.

3.1 Refractive index of air

The refractive index of the media (n) affects the laser wavelength in that media (λ)

(3) $$\lambda = \frac{\lambda_0}{n}.$$

where λ_0 is the vacuum wavelength of the laser beam.

The vacuum wavelength can be determined with a very small uncertainty; therefore the main uncertainty component in interferometric measurements is the refractive index of air. Most laser interferometric measurements are carried out in ambient air, thus the refractive index of air has to be known accurately in length metrology. The index depends on pressure, temperature and composition of the air.

The refractive index of air can be determined in several different ways. In typical length measurements, it is calculated using the (updated) Edlén formula [18, 19, 20, 21] and measured pressure, temperature and humidity. In laboratory conditions pressure and humidity can be measured accurately enough with barometers and hygrometers. Measurement of the temperature is more difficult because there can be large temperature gradients and sudden changes. Therefore, in demanding measurement conditions new methods are needed to measure the refractive index along the interferometer measurement path. An acoustic method developed in this thesis [IV, 22] and a spectroscopic method [23, 24] can be used to measure effective temperature along the beam path. The acoustic method is useful for short distances from centimetres to metres with sub-nanometre uncertainty, spectroscopic measurement for long distance measurements of over 100 metres. Two-colour interferometry can be used to compensate for the refractive index directly [25, 26, 27]. The refractive index can also be measured directly with refractometers [28, 29, 30], but the measurement is not along the interferometer beam path.

3.1.1 Acoustic method for determination of the refractive index of air

Temperature changes may be fast and local, and they are very difficult to measure with conventional temperature sensors. Even in quite stable industrial conditions, the temperature gradients can be several degrees. A new method for determination of the

effective air temperature and the refractive index of air was invented by Leonid Mihaljov, and further developed and validated in this thesis [V]. The method is based on measurement of the speed of ultrasound. It was first developed for longer distance measurements (up to 11 m) in a one-dimensional (1-D) setup. The method was further developed for two-dimensional (2-D) setups with plane mirror interferometers and shorter distances (from 50 mm to 500 mm) [31]. The 2-D method was developed especially for measurements with sub-nanometre uncertainty, e.g. in the semiconductor industry.

The speed of sound in air is about 2000 times more sensitive to temperature changes than the refractive index of air. This is exploited in the method developed for the measurement of the effective temperature and refractive index along the interferometer beam path.

3.1.1.1 Equations

In paper V, equations for temperature and the refractive index of air as a function of speed of ultrasound, pressure, humidity and CO_2 concentration were fitted. The equations are based on our measurements of the speed of sound of a 50 kHz ultrasound burst, the Cramer equation [32] and dispersion correction [33, 34] on the speed of sound, and the equation for the refractive index on the Edlén formula [19]. Standard uncertainties of the equations are 15 mK for temperature and 1.7×10^{-8} for the refractive index. Similar equations are developed for 400 kHz ultrasound for the 2-D setup.

3.1.1.2 Setup

The test setup for 1-D measurements (Figure 2) was designed at MIKES as part of this thesis. The setup for 2-D measurements (Figure 3) was developed by AcWaCo Ltd.

A short ultrasound burst is sent and received by acoustic piezo transducers (APTs). The speed of sound is calculated from the measured time of flight and the distance is measured by a laser interferometer. Two pairs of piezo transducers are placed symmetrically around the laser beam to avoid Abbe error (see 4.2 and Figure 13). The time of flight of a short ultrasound burst is transmitted by each APT in turn and received by the facing APT. In the 2-D setup plane mirror interferometers are used. Because the mirrors are moving in 2-D, the transducers cannot be mounted face to face but are mounted side by side and the ultrasound burst echoed from the mirror is measured.

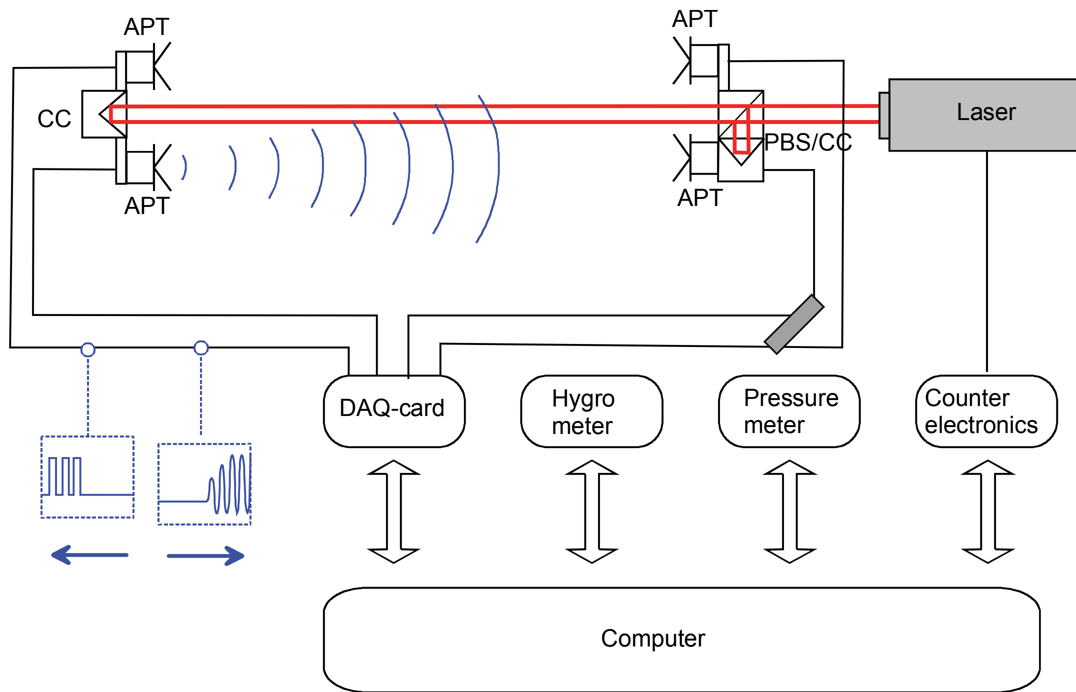

Figure 2 *Measurement setup for refractive index measurement in 1-D configuration. PBS is polarizing beam splitter, CC corner cube and APT acoustic piezo transducer.*

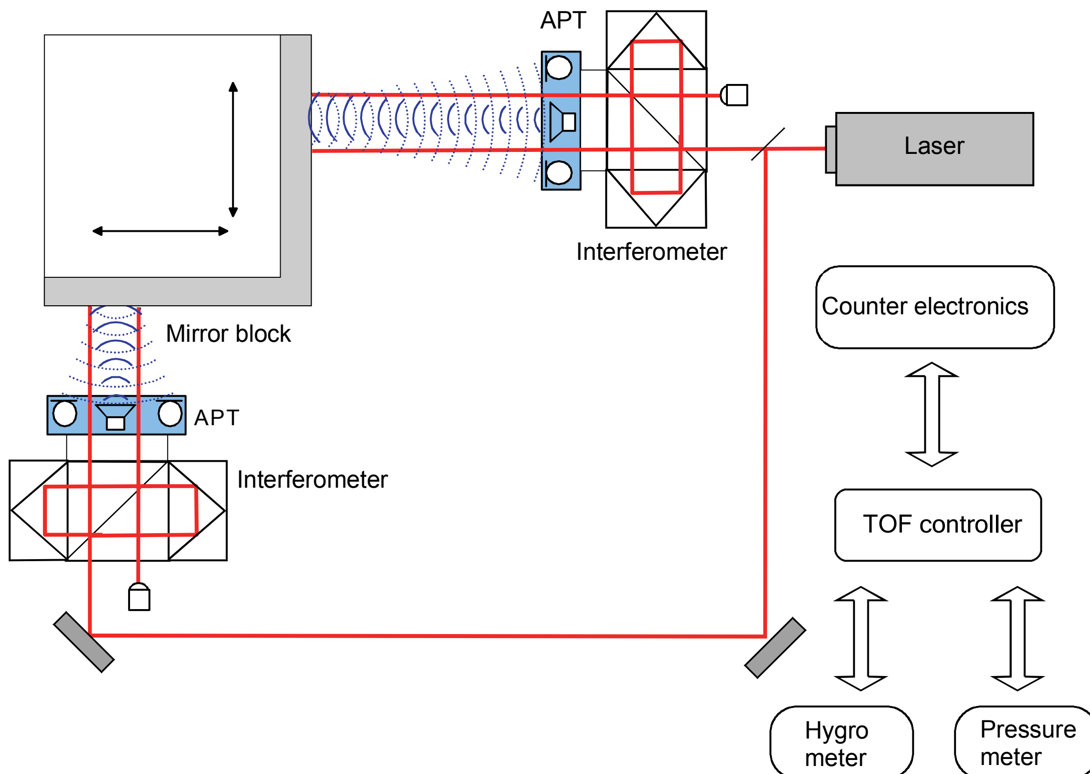

Figure 3 *Measurement setup for refractive index measurement in 2-D configuration. APT is acoustic piezo transducer and TOF time of flight.*

3.1.1.3 Results

The method was simulated in different environments. Demanding measurement conditions e.g. in workshops were simulated by exposing the beam path to a turbulent warm airflow. Warm turbulent air causes rapid, wide variations of local temperature that are very hard to compensate for. In the measurement shown in Figure 4, a fixed distance was measured using a laser interferometer, and the measurement was disturbed by blowing warm air across the beam path. The maximum temperature of the airflow was ~25°C and changes in average temperature along the laser beam path were up to 0.8°C. The changes in interferometrically measured distance were ~0.8 µm/m in the uncompensated distance, but only ~0.05 µm/m in the acoustically compensated distance. The slight increasing trend in compensated distance was caused by thermal expansion of materials, which could not be wholly avoided during measurement. Small peaks in the compensated distance were caused by imperfect synchronisation of the time of flight and distance measurements.

Standard uncertainties for measured temperature and refractive index are 25 mK and 2.6×10^{-8} for a distance of 5 m.

The speed of sound is related to the velocity of the media, such as airflow. Sensitivity of the setup to axial airflow was therefore examined. In the measurement shown in Figure 5, the acoustic measurement was disturbed by airflow caused by two fans operated in turn. The maximum airflow was ~0.2 m/s, and the direction of the airflow was changed several times. The speeds of sound measured with each acoustic transducer in turn are shown in Figure 5a. The airflow effect is clearly visible, but could be eliminated by taking an average of the speeds measured in both directions. Most variations in the average speed of sound were caused by small temperature variations (~50 mK), and their effect on the refractive index and interferometrically measured distance could be compensated for (see Figure 5b).

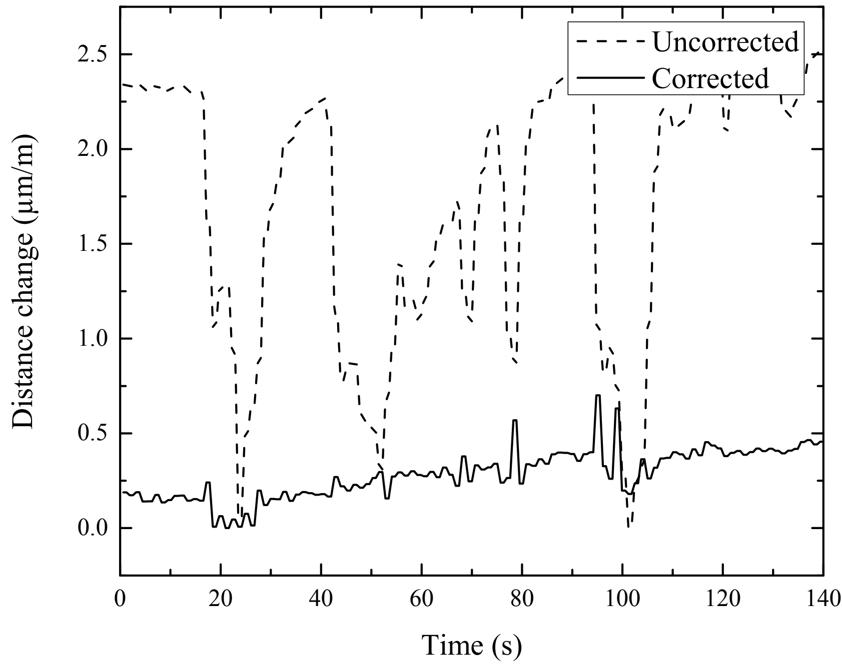

Figure 4 *Effect of warm airflow on interferometric measurement. Changes in interferometrically measured distance (uncorrected ----- and acoustically corrected ——). The total distance in the measurement was ~2.9 m*

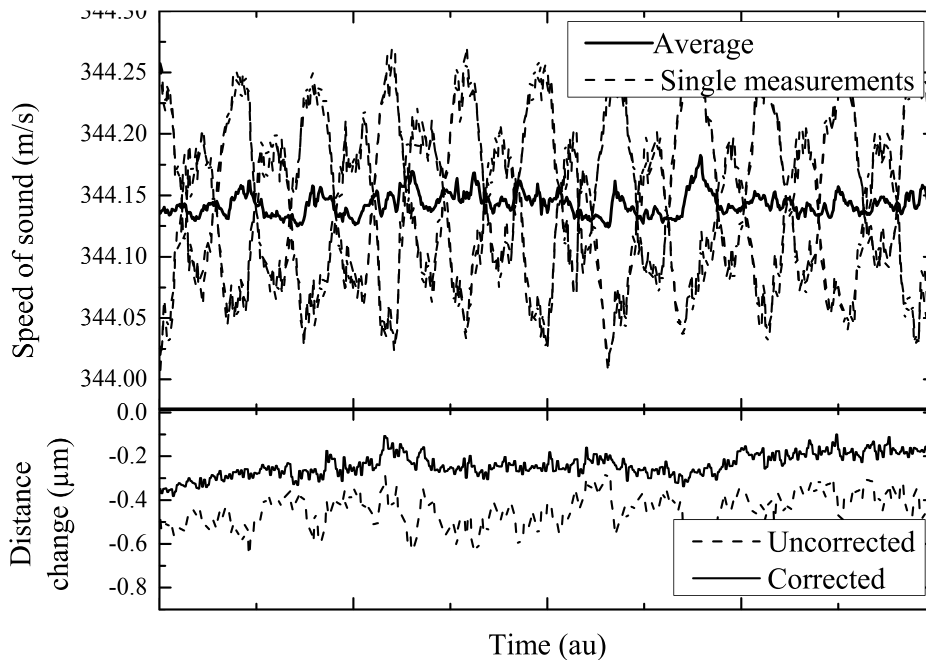

Figure 5 *Effect of airflow on acoustic measurement. Top: speed of sound measured with each of the transducers (----) and averaged (——). Bottom: uncorrected (----) and acoustically corrected (——) interferometrically measured distance.*

The method was tested against a vacuum interferometer at PTB as part of the Euromet 744 project. The agreement between measurements of the refractive index was at a level of 10^{-7}. Temperature variations were well compensated for, but a difference between absolute temperature and refractive index were seen in the measurements. Differences between the refractive index calculated from the reference temperature, pressure and humidity, and the acoustically measured refractive index are shown in Figure 6. The agreement with the results was not as good as expected, but an uncertainty level of 10^{-7} is still good in industrial conditions, and better than can be achieved with traditional temperature sensors. In most interferometric measurements, compensation of temperature changes is more important than measurement of absolute temperature. For this purpose the method was found to be sufficiently accurate.

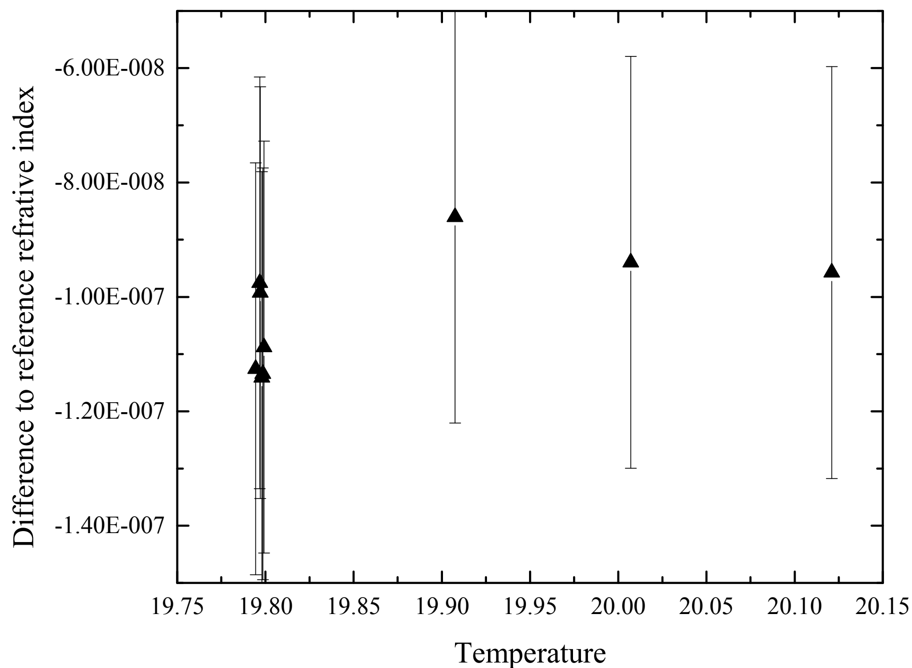

Figure 6 *Differences between the refractive index of air calculated with Edlén formulae and the refractive index measured acoustically.*

3.2 Interferometer periodic nonlinearity

The laser interferometer is an accurate method for length measurements when counting integer numbers of interferometer fringes. Usually red He-Ne lasers at 633 nm are used, i.e. the fringe distance is usually 316.5 nm or 158.25 nm. Therefore, phase detection of the interferometer signal is needed in nanometre scale measurements. Due to unideal optics, imperfectly polarized laser beams and imperfect phase detection, there are small periodic nonlinearities in the interferometric measurement [35, 36, 37, 38].

There are several different methods for detecting and correcting the nonlinearity. In heterodyne interferometers an external reference can be used to directly measure together all the effects causing periodic nonlinearity of the detected phase. The reference can be the time index of the interferometer samples with a smooth movement assumption [39], a capacitive distance sensor [e.g. [40, 41]], a pressure cell, which has also been used for varying the optical path length [37], or another interferometer using different wavelength such as an x-ray interferometer [42]. Additional optics, electronics and detectors can be used to correct some part of the optical nonideality [43]. Multipass interferometry is a new method for accurate phase measurement [44, 45]. The Heydemann correction is generally used in the correction of nonlinearity of homodyne interferometers [46, 47].

3.2.1 Method

A new method for the correction of nonlinearity has been developed as part of the MIKES interferometrically traceable metrological AFM (IT-MAFM) project [II, 48]. A capacitive sensor is used for the measurement of nonlinearity, which in a capacitive sensor is slowly changing and is not a periodic function of the position. The capacitive sensor is calibrated using calibration steps that equal the fringe distance of the interferometer, i.e. the phase of the interferometer signal is the same at all measurement points. This eliminates the interferometer nonlinearity. Then the interferometer nonlinearity is measured using sub-fringe stepping. A correction vector is calculated as a function of the phase.

The algorithm is included in the measurement software of the MIKES IT-MAFM and the correction vector can be measured before the AFM measurements. The correction is done online.

3.2.2 Setup and measurements

A test setup for the nonlinearity measurements included a piezo stage (Queensgate NPS-Z-15H) with integrated capacitive sensors, and a double-pass heterodyne plane mirror interferometer (Zygo 2000) was designed. The same components are used in the IT-MAFM setup [II]. Nonlinearity of the capacitive sensors was measured using an interferometer with a step length of 158.25 nm over a 15 μm range. Next the non-linearity of the laser interferometer was measured using a step size of 1.58 nm; the measurement was repeated 30 times.

3.2.3 Results

After careful adjustment, the nonlinearity of the laser interferometer in the test setup was found to be about 0.3 nm. The nonlinearity correction vector as a function of phase is shown in Figure 7. The differences between the positions measured by the capacitive

sensor and by the laser interferometer with and without nonlinearity correction are shown in Figure 8. The variations in the corrected data are about 0.1 nm.

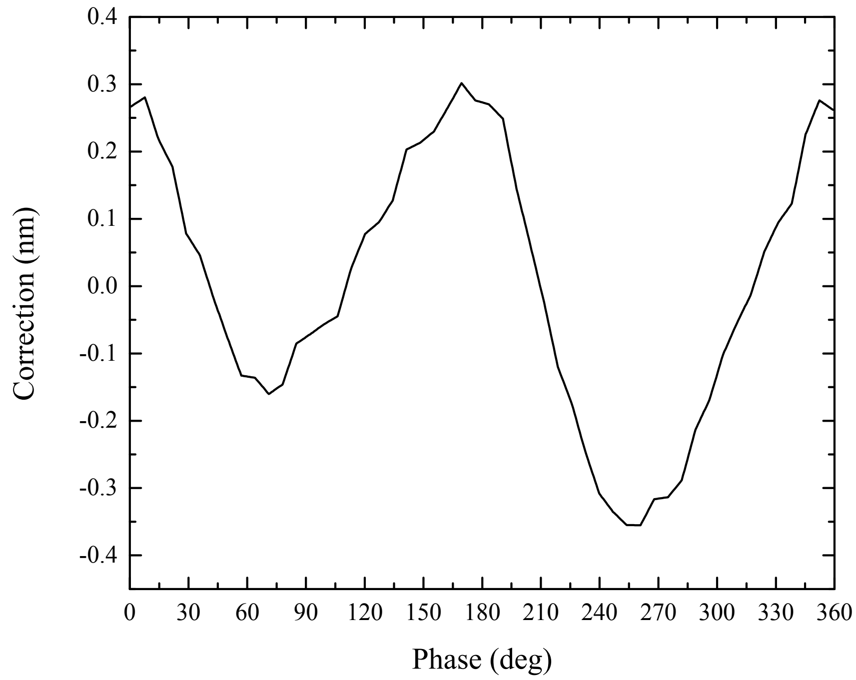

Figure 7 *Nonlinearity correction vector for laser interferometer nonlinearity used in Figure 8*

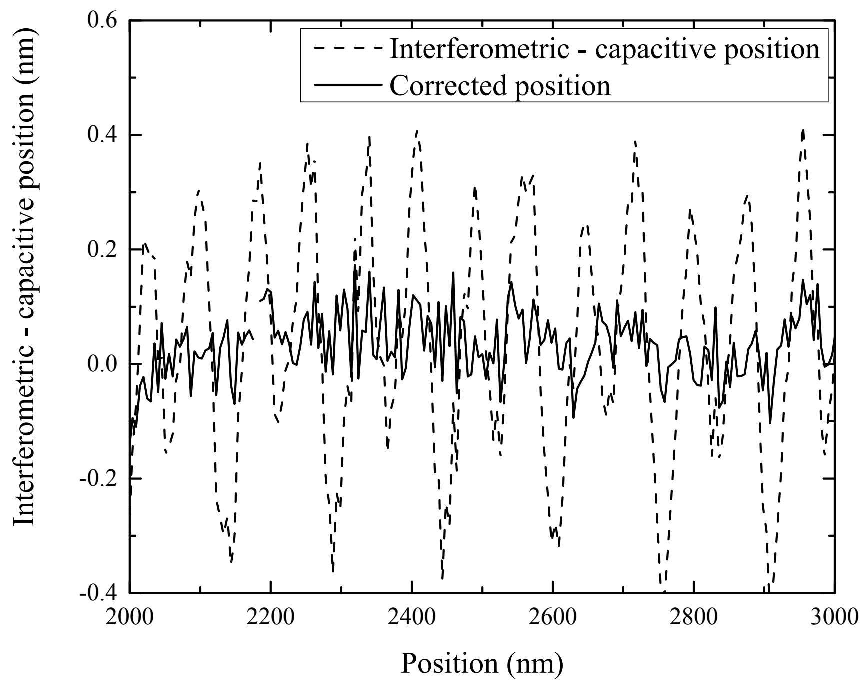

Figure 8 *Differences between capacitively and interferometrically measured position —— with and ----- without non-linearity correction.*

During the AFM measurement, the nonlinearity can be corrected online. In the IT-MAFM the nonlinearity is 0.2 nm – 0.8 nm and after the correction below the noise level. The effect of the non-corrected interferometer nonlinearity can be clearly seen in the MAFM topography measurement if the sample is slightly tilted. The effect is clearly seen when measuring a flat sample. Artificial periodic structures caused by the nonlinearity can be seen in the measured topography. As an example, a measurement of a flatness standard with and without nonlinearity correction is shown in Figure 9. The diagonal stripes in the right image are caused by the nonlinearity of the interferometer.

Although the periodic nonlinearity is a systematic error component, it has been observed to change over time [43, 49, 50]. In the IT-MAFM the nonlinearity is found to be stable at least for a few days in stable measurement conditions. Measurement of the nonlinearity is easily repeated, and can be done before each measurement if a really high accuracy is needed.

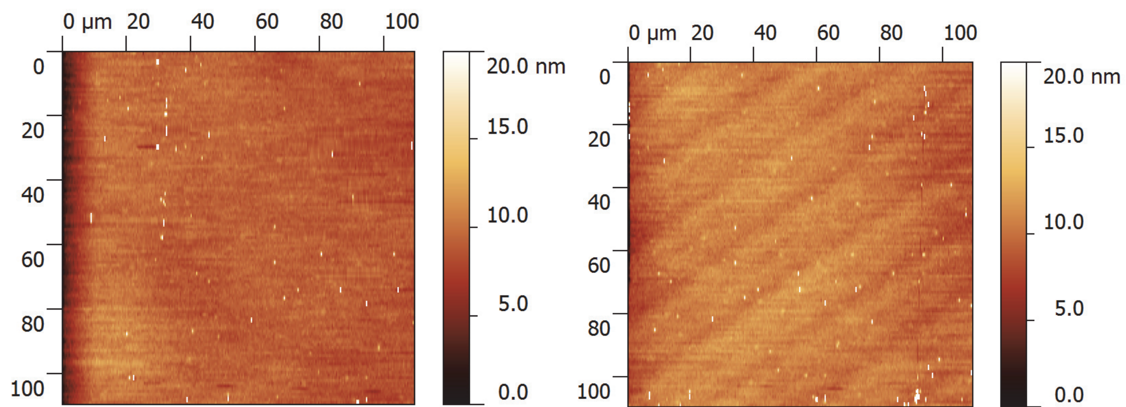

Figure 9 *AFM topography measured with (left) and without (right) correction of nonlinearity of the laser interferometer.*

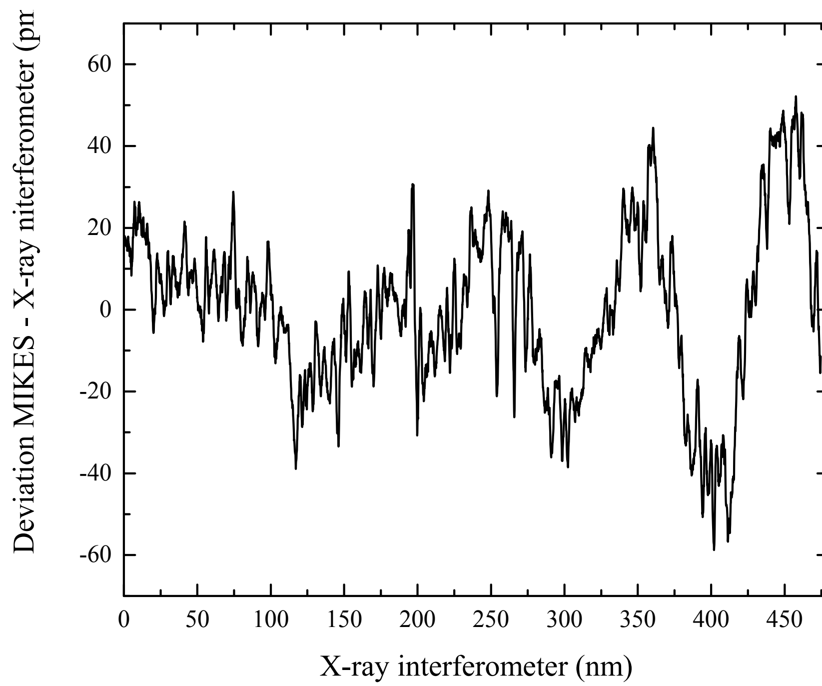

Figure 10 *Difference between the MIKES method and NPL x-ray interferometer.*

The nonlinearity correction method was further developed and compared against an x-ray interferometer at NPL as part of the NANOTRACE project [51, 52]. The uncorrected nonlinearity was 300 pm and after correction the rms residual error was 14 pm. The difference between the x-ray interferometer and nonlinearity-corrected interferometer is shown in Figure 10.

4 Scanning probe microscopy

Scanning probe microscopes (SPMs) are versatile tools for nanometre scale measurements. The first type of SPM, a scanning tunnelling microscope (STM), was developed by Binning and Rohrer in 1982 [53], earning them a share of the Nobel Prize for physics in 1986. In the STM, the detected tip-sample interaction is based on a quantum mechanical tunnelling effect between the tip and the sample. The first atomic force microscope (AFM) was developed by Binning and Quate in 1986 [54]. In AFMs, the detection of surface topography is based on Van der Waals forces between the atoms on the surface and those at the apex of the measurement tip. In addition to the sample topography, other properties can be measured such as electrostatic (electrostatic force microscopy, EFM) or magnetic (magnetic force microscopy, MFM) interactions.

The terminology is sometimes confusing. In addition to the term AFM, the term scanning force microscope (SFM) is also used, or SPM is used only to mean AFM. In this thesis only AFM is generally used, but SPM is used when the results can be generalized to other types of SPMs.

AFMs fall into in three categories depending on the quality of the position measurement system: open loop, closed loop, or metrological AFMs. Different axes of the AFM can be of different types, e.g. metrological in X and Y, but open or closed loop in Z. Even one instrument can have different measurement modes to be selected from depending on the required accuracy, noise level and measurement time. [55, 56]

In open loop AFMs the position measurement comes directly from the piezo driving voltage without feedback. Open loop AFMs are typically older or lower priced instruments. Calibration might be needed before and after each measurement.

Closed loop AFMs have position feedback from position sensors in the XY directions, and position measurement by a position sensor in the Z direction. The calibration interval depends on the required accuracy and stability of the position sensors.

The most accurate type of AFM is metrological AFMs (MAFMs), which have position measurement with integrated laser interferometers. The interferometric position measurement is directly traceable to the metre via the laser wavelength (see Chapter 3).

MAFMs have been developed at many NMIs. The first AFMs that were metrological in all three dimensions were developed more than 10 years ago at PTB (Germany) [60] and AIST (Japan) [63]; in the XY dimensions at NIST (USA) [67], and in 1-D at METAS (Switzerland) [69]. Since then, leading NMIs have developed second or third generation MAFMs, smaller NMIs and some universities have been working on MAFM development [II, 57, 58, 59, 72, 82], and there are several ongoing MAFM projects [74, 75, 78, 80, 81]. Metrological AFMs developed in different countries are listed in Table 1. The bases of the design are different; many laboratories have selected the same approach as MIKES, with a commercial AFM head [76], scanner stages [76, 80 81] and/or interferometers. Some laboratories have developed their own scanner systems with non-orthogonal but symmetric movements related to the AFM probe [74, 78]. A quartz tuning fork AFM head [80, 81] can be used instead of an AFM head with optical detection of the cantilever deflection. Some instruments are based on a commercially available nanomeasuring

machine (NMM) by SIOS [62, 73]. The scan ranges of the MAFMs vary from a typical AFM scan range (< 100 µm) to a long range of up to several millimetres.

Table 1. *MAFMs in different NMIs and examples of standard uncertainty estimates for pitch p=300 nm and/or step height h=1000 nm.*

Country	NMI		Type	Range	Uncertainty u_c	Ref
Finland	MIKES	IT-MAFM	3-D metrological	100 × 100 × 16 μm^3	uc(p) = 0.022 nm[e] uc(h) = 0.55 nm[e] uc(h) = 0.56 nm*	II
Germany	PTB	Veritek B	3-D metrological	70 × 15 × 15 μm^3		60
		Veritek C	3-D metrological	70 × 15 × 15 μm^3	uc(h)=0.62 nm[d]	61
		LR	3-D metrological	25 × 25 × 5 mm^3	uc(p) =0.0054 nm[c] uc(p) =0.0085 nm[e] uc(h) =0.57 nm[d] uc(h) =0.6 nm[e] uc(p) = 0.56 nm*	62
Japan	AIST	Nanometrological AFM	3-D metrological	17.5 × 17.5 × 2.5 μm^3	uc(p) = 0.49 nm[c] uc(h) = 0.705 nm[a]	63
		DLI-AFM	3-D metrological	100 × 100 × 12 μm^3	uc(p) = 0.007 nm*	64
USA	NIST	M^3	XY metrological	50 × 50 mm^2	uc(p) = 1.5 nm*	65, 66
		C-AFM	XY metrological Z capacitive gauge calibrated interferometrically offline	50 × 50 μm^2	uc(p) = 0.36 nm[b] uc(p) = 0.2 nm[c] uc(h) = 2.5 nm[a]	67, 68
Singapore	A*STAR	LRM-AFM	3-D metrological	25 × 25 × 5 mm^3	uc(p) = 0.36 nm[b] uc(p) =0.2 nm[c] uc(p) = 0.18 nm* uc(h) = 0.9 nm[a,e,*]	
Switzerland	METAS		X and Z metrological	380 × 70 × 7 μm^3	uc(p) =0.006 nm[b] uc(p) = 0.074 nm[c] uc(p) = 0.0075 nm* uc(h) = 0.65 nm[a] uc(h) = 0.75 nm*	69
			3-D metrological			
UK	NPL		3-D metrological		uc(p) = 0.4 nm[c] uc(h) = 2.61 nm[a]	70
Korea	KRISS		XY metrological	100 × 100 × 12 μm^3	uc(p) = 0.094 nm[d]	71

			Z capacitive gauge			
Italy	INRIM		XY interferometric Z capacitive gauge	30 × 30 × 18 μm^3	uc(p) = 1 nm [c,e] uc(p) = 1 nm* uc(h) = 1.3 nm [e]	72
China	NIM	NMM	3-D metrological	50 × 50 × 2 mm^3	uc(h)= 2 nm[a]	73
Netherlands	VSL		3-D metrological			74 75
Belgium			3-D metrological			76 77
France	LNE		3-D metrological	60 × 60 × 15 μm^3		78 79
Canada	NRC		3-D metrological			80
Australia	NMIA		3-D metrological			81
Russia	VNIIM				uc(p) = 0.2 nm[c] uc(p) = 0.15 nm* uc(h) = 0.81 nm*	
Czech Republic	CMI		3-D metrological	1 × 1 cm^2 × 35 µm	uc(p)= 0.9 nm[e] uc(h) = 8.2 nm[5]	82
Denmark	DFM		Closed loop		uc(p) = 0.072 nmc uc(h) = 4.4 nma uc(p) = 0.29 nm* uc(h) = 1.4 nm*	

* CMC database
[a] NANO2 comparison [7]
[b] NANO4 comparison [5]
[c] NANO5 comparison [6]
[d] Euromet 707 comparison [8]
[e] Euramet 925 comparison [4]

4.1 Traceability of SPM measurements

The main purpose of this thesis it to establish a traceability chain for nanometre scale measurement. The traceability chain for nanometre scale measurements in Finland is shown in Figure 11. The chain starts with the definition and realization of the metre (see Chapter 3). The vacuum wavelengths of the lasers used in interferometric or diffraction measurements are calibrated against an iodine-stabilised He-Ne laser whose frequency is measured with a frequency comb [83]. Transfer standards are calibrated by an IT-MAFM or a laser diffraction setup using the calibrated wavelength of the laser as a link to the realization of the metre. The calibrated transfer standards can then be used in calibration of SPMs to achieve traceability of SPM measurements in industry and research institutes. Temperature, pressure and humidity measurements are used for determination of the

refractive index of air and for the correction for thermal expansion. These measurements are traceable to the national standards at MIKES.

A widely used traceable measurement method is substitution measurement. In substitution measurements, e.g. before and after actual measurements of the sample, relevant scales are checked by measuring the calibrated pitch or the step height of a standard. Specific software [e.q. 84, 85] can be used to correct the sample data according to the results of the transfer standard. This is a fast and accurate method for many purposes, but leaves several properties of the SPM uncovered. The substitution method was used in the measurements of the NANO5 comparison for 2-D gratings at MIKES [6].

Another approach for SPM traceability is characterization of the metrological properties of a measurement instrument. The instrument errors are calibrated and corrected in a way that allows calculation of uncertainty of the co-ordinate system at any position of the scanner. This approach is more demanding than the substitution method, but gives a better understanding of the metrological properties of the instrument and allows more degrees of freedom regarding the sizes and shapes of the measured calibration features. This kind of characterization was done for the IT-MAFM in paper II and for a commercial AFM in paper IV. Methods for the 3-D calibration of AFMs have been developed elsewhere [86].

A third approach is a combination of the other two. The scales and possibly other properties of the instrument are calibrated and the substitution method is used when high accuracy is needed. This requires less work than full characterization, but the user should be aware of the limitations of partial calibration.

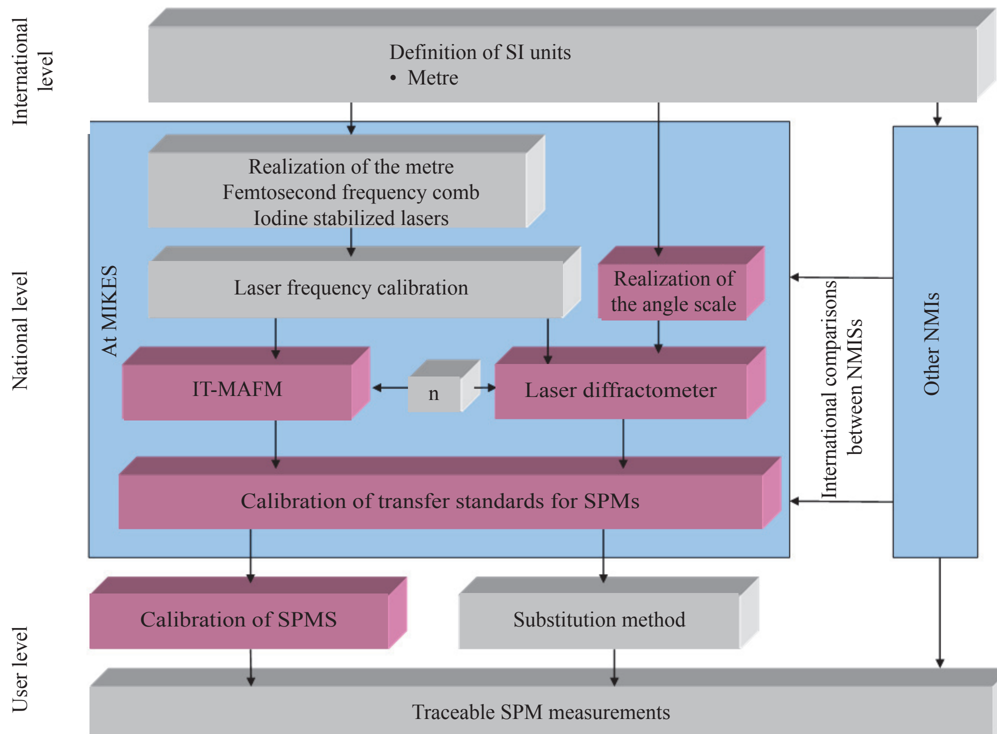

Figure 11 *Traceability chain for SPM measurements.*

4.2 Calibration principles of SPMs

Calibration of an SPM involves calibration of the X, Y and Z scales, but also measurements and correction of orthogonality errors between the axes, angular errors in the movements and out-of-plane movements. There are several other error types that affect measurement and have to be taken into account when evaluating the uncertainty. Some typical error sources are shown in Figure 12. Many of the error sources are case-specific and must be estimated for each measurement separately.

There are other error sources that are difficult or impossible to compensate for with calibration, but must be taken into account in the uncertainty budget of actual measurements. These include tip shape, tip wear, tip-sample effects, temperature changes, drifts, contamination of the sample, turbulence of air, vibration and signal noise. Also the scan rate, scan range and other settings might affect the calibration and measurement results.

There are several different types of calibration standards that can be used to calibrate an SPM. The X and Y scales and nonlinearities of the scales can be calibrated using 1-D or 2-D gratings. The selected grating pitch depends on the measurement range. A 2-D grating can be used to calibrate the orthogonality error between the X and Y axes. The Z scale can be calibrated using step height standard. Several different steps are needed for calibration of the full scale. Nonlinearity of the Z scale is difficult to calibrate but can be at least partly detected if the measurements of the steps are repeated in different positions of the measurement range. Orthogonality of the Z axis can be measured using a triangular grating [87]. There are also calibration standards with pyramidal structures that can be used to calibrate the X, Y and Z scales, linearities and orthogonalities in only one measurement [88]. In most measurement software, the calibration correction, at least scale correction, can be done online during the measurement, or offline using self-made, commercial (e.g. SPIP [84]) or open source (e.g. Gwyddion [85]) software.

1-D and 2-D grating standards down to about 300 nm are generally commercially available. 1-D standards have been developed down to 25 nm pitch [89, 90, 91, 92]. The PTB and NanoScale Organizing Committee maintain a list of available standards [93].

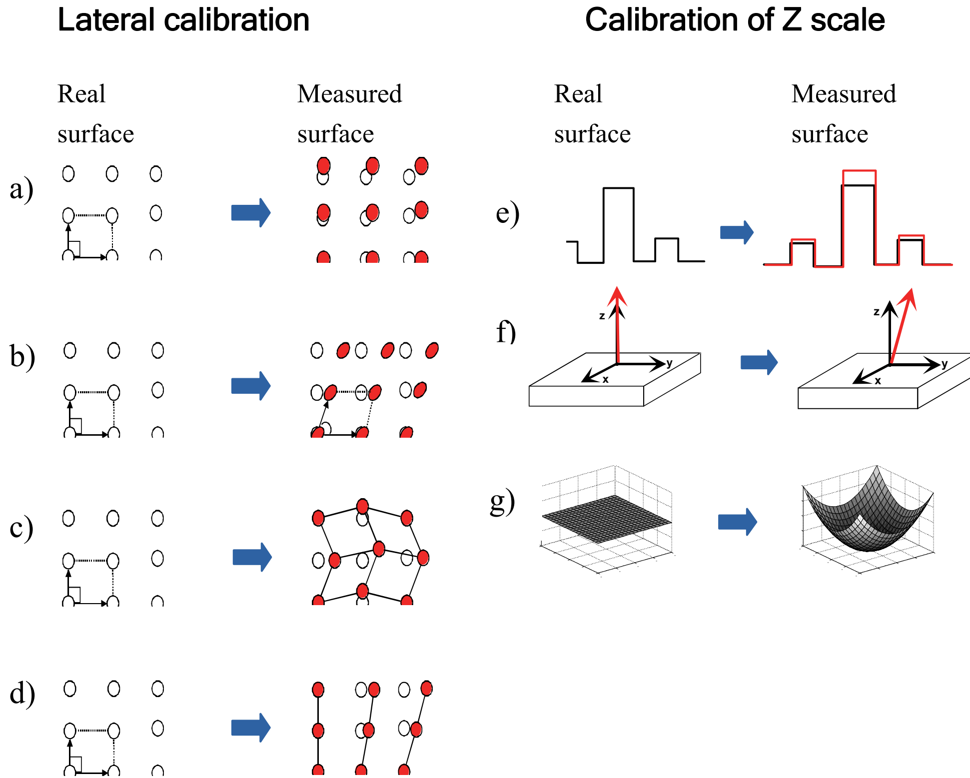

Figure 12 *Error types of SPMs requiring calibration: a) X and Y scale errors; b) orthogonality error; c) and d) guidance errors or angular errors; e) Z scale errors; f) orthogonality of the Z axis; g) out-of-plane errors.*

Scale correction (C) for X and Y axes can be measured with 1-D or 2-D calibration gratings. A simple method for determination of the scale correction factor is to measure the grid perpendicular to the calibrated axis over n pitches, measure the distance (l_k) from one edge to another, and compare the distance to the known dimensions of the standard (P_{cal}, taken from the calibration certificate):

(4) $$C = \frac{kP_{cal}}{l_k} \quad .$$

The orthogonality of the X and Y axes can be measured using a 2-D calibration standard and error separation method. The measurements are done in two perpendicular orientations. Orthogonality errors of the AFM (γ_{xy} - 90°) and the sample (γ_s - 90°) can be calculated from the equations

(5)
$$\gamma_{xy} - 90° = \frac{(\gamma_0 - 90°) + (\gamma_{90} - 90°)}{2}$$
$$\gamma_s - 90° = \frac{(\gamma_0 - 90°) - (\gamma_{90} - 90°)}{2},$$

in which γ_0 and γ_{90} are angles between the horizontal and vertical pitch directions (the directions are fixed to the AFM, i.e. the co-ordinate system is not rotating with the sample) in different sample orientations (0° and 90°, respectively). Orthogonality of the Z axis can be measured using a triangular grating and error separation method [87]

The typical geometrical errors – Abbe [94] and cosine errors – must be taken into account when calibrating SPMs and in SPM measurements. The Abbe error is caused by an angular error in movements $\delta\alpha$, and the Abbe offset δy (see Figure 13). It can be minimized by following the Abbe principle, i.e. by minimizing the Abbe offset. Abbe errors can be corrected if the Abbe offset and angular errors are known.

(6)
$$\delta l_{Abbe} = \delta y \sin(\delta\alpha).$$

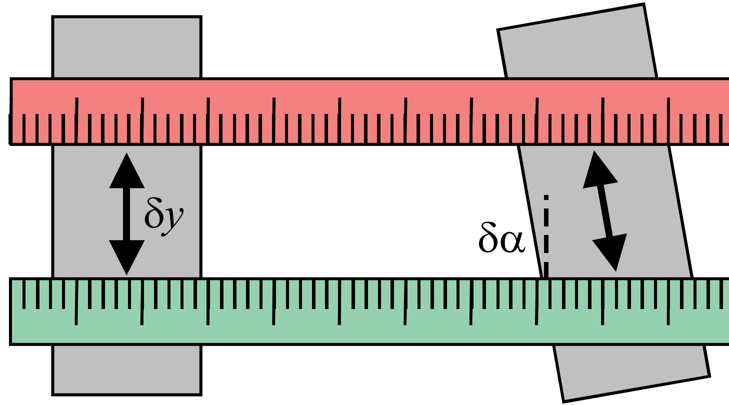

Figure 13 *Abbe error caused by angle error in movements $\delta\alpha$ and Abbe offset δy.*

A large Abbe error typically occurs in SPM measurements when the calibration standard and measured sample are of different height, or the sample is moving under a measurement probe. As shown in papers II, III and IV, this can occur even in a well-aligned measurement system.

Cosine errors are caused by misalignments in scale, movement or measurement target. In SPM measurement, typical causes of cosine errors are sample tilt and other errors in sample alignment (Figure 14). AFM samples are usually slightly tilted and the tilt is corrected by plane correction. Plane correction is not a rotation but a projection, which causes cosine error in the measurement (Figure 15).

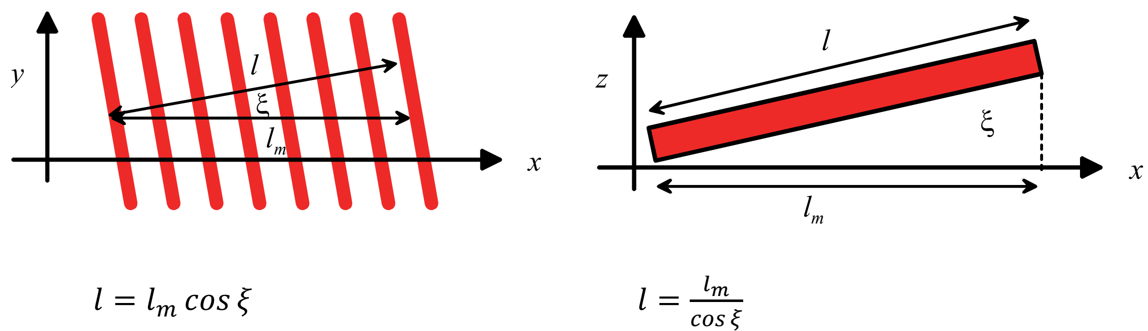

Figure 14 *Typical cosine errors in SPM measurement: A rotational error in the sample alignment, and tilt of the sample.*

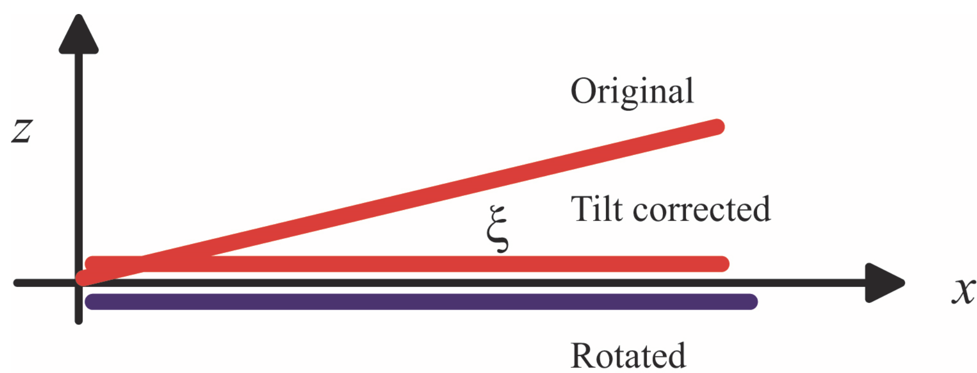

Figure 15 *Cosine error in tilt corrected AFM topography compared to a rotated one.*

4.3 MIKES metrological AFM

The interferometrically traceable metrological AFM (IT-MAFM) is part of the traceability chain for nanometre scale measurements. The main purpose of the equipment is the calibration of transfer standards for SPMs, but it can also be used in other measurements requiring a high level of accuracy. Characterization of the metrological properties and uncertainty estimations were a crucial part of the development project.

4.3.1 Setup

The IT-MAFM consists of 3-D interferometers, a PSIA XE-100 AFM head and a 3-D scanner stage. There is an optical microscope and mechanics for the sample alignment, stepper motors for tip approach, environmental sensors for temperature, pressure and humidity, and controllers for all instruments. Two computers are used for the measurement control and data acquisition.

The main design principles were elimination or reduction of known error sources and external disturbances. The design is a reasoned compromise on high accuracy, usability and cost efficiency.

The interferometric position measurement follows the Abbe principle. The AFM measurement tip is located at the crossing point of the measurement lines of the 3-D interferometers. The X and Y interferometers use differential optics. The refractive index of air is corrected using the Edlén formula [19] and measured temperature, pressure and humidity.

Thermal stability is important, because temperature changes are the main source of mechanical drift during the measurement. The laboratory is thermally stabilized. The measurement chamber is thermally and acoustically insulated and there is a small thermally stabilized airflow inside the chamber. The effect of thermal expansion is minimized using Invar and Super Invar alloys in the metrology frame. There are four temperature sensors in the measurement chamber, and the temperature can be recorded during stabilization and measurement.

Vibrations and acoustic noise are minimized using dampers under the table, in inlet and outlet air channels, and with plastic shielding around the measurement area. The effect of noise is reduced through careful selection of averaging times in the interferometer reading. The symmetric design and a 25 mm invar base plate reduce vibrations in the metrology frame.

4.3.2 Measurement principle

The sample position is measured by laser interferometers in all three dimensions. Other measurement modes can be used to reduce measurement time and noise. When calibrating 1-D and 2-D gratings, traceable scales are needed only in the X and Y directions and a capacitive measurement can be used in the Z direction. For step height calibration a traceable scale is needed in the Z direction, but capacitive position measurement can be used in the X and Y directions.

Scanning strategies for shortening the measurement time include skipping of measurement points in areas of little or no interest [III]. In step height calibration or other measurement of regular structures, scanning speed can be adjusted to increase across flat areas and slow down when approaching an edge [III].

4.3.3 Traceability and uncertainty of the IT-MAFM

Interferometric position measurement with calibrated laser wavelength, traceably measured refractive index and carefully characterized instrument errors give traceability to the coordinate system.

In the model function for a measurement point $\mathbf{r}=[x,\ y,\ z]$, correction for non orthogonal X, Y and Z axes **C,** and Abbe errors **A,** are approximated to be linear functions of the interferometrically measured coordinates $\mathbf{m} = [x_m,\ y_m,\ z_m]$. Error components independent of the measured position are included in **D**.

(7) $$\mathbf{r} = (\mathbf{C} + \mathbf{A})\mathbf{m} + \mathbf{D} \,.$$

In addition to equation (2), the equation for the measured coordinates includes the correction for interferometer nonlinearity $\delta\varphi_{nonlin,x}$

(8) $$x_m = \frac{\left(k_x + \delta\varphi_{nonlin,x}\right)\lambda_0}{n_x} \,.$$

and respectively for y_m and z_m. k_x denotes the counter readings (integer + phase) of interferometer fringes, λ_0 the vacuum wavelength of the laser light, and n_x the refractive index of air along the X axis.

The matrix **C** corrects the error caused by non-orthogonal X, Y and Z axes.

(9) $$\mathbf{C} = \begin{pmatrix} 1 & 0 & 0 \\ \dfrac{\cos\gamma_{xy}}{\sin\gamma_{xy}} & \dfrac{1}{\sin\gamma_{xy}} & 0 \\ s\left(\dfrac{\cos\gamma_{xy}}{\sin^2\gamma_{xy}}\left(\cos\gamma_{yz} - \cos\gamma_{xy}\cos\gamma_{xz}\right) - \cos\gamma_{xz}\right) & \dfrac{s}{\sin^2\gamma_{xy}}\left(\cos\gamma_{xy}\cos\gamma_{xz} - \cos\gamma_{yz}\right) & s \end{pmatrix}$$

where

(10) $$s = \left(1 - \cos^2\gamma_{xz} - \left(\frac{\cos\gamma_{yz} - \cos\gamma_{xy}\cos\gamma_{xz}}{\sin\gamma_{xy}}\right)^2\right)$$

and the γs are angles between the axes.

The angular positions $\alpha(x)$ at certain coordinates x are approximated as linear functions of coordinates x, y and z:

(11) $$\alpha(x) = \frac{\Delta\alpha_x}{\Delta X} x .$$

$\Delta\alpha_x$ is the angular error for movement in the X direction across the whole range ΔX of the stage. Because the angle values are small, sinα ≈ α (α in rad). Linear approximation of the Abbe errors (see equation 6) for a 3D measurement is expressed as matrix **A**.

(12) $$\mathbf{A} = \begin{pmatrix} \delta z_0 \frac{\Delta\alpha_{pitch,x}}{\Delta X} + \delta y_0 \frac{\Delta\alpha_{yaw,x}}{\Delta X} & \delta z_0 \frac{\Delta\alpha_{pitch,y}}{\Delta Y} + \delta y_0 \frac{\Delta\alpha_{yaw,y}}{\Delta Y} & \delta z_0 \frac{\Delta\alpha_{pitch,z}}{\Delta Z} + \delta y_0 \frac{\Delta\alpha_{yaw,z}}{\Delta Z} \\ \delta x_0 \frac{\Delta\alpha_{roll,x}}{\Delta X} + \delta z_0 \frac{\Delta\alpha_{pitch,x}}{\Delta X} & \delta x_0 \frac{\Delta\alpha_{roll,y}}{\Delta Y} + \delta z_0 \frac{\Delta\alpha_{pitch,y}}{\Delta Y} & \delta x_0 \frac{\Delta\alpha_{roll,z}}{\Delta Z} + \delta z_0 \frac{\Delta\alpha_{pitch,z}}{\Delta Z} \\ \delta x_0 \frac{\Delta\alpha_{roll,x}}{\Delta X} + \delta y_0 \frac{\Delta\alpha_{yaw,x}}{\Delta X} & \delta x_0 \frac{\Delta\alpha_{roll,y}}{\Delta Y} + \delta y_0 \frac{\Delta\alpha_{yaw,y}}{\Delta Y} & \delta x_0 \frac{\Delta\alpha_{roll,z}}{\Delta Z} + \delta y_0 \frac{\Delta\alpha_{yaw,z}}{\Delta Z} \end{pmatrix}$$

where δy_0 and δz_0 are uncertainties of the Abbe offsets in the Y and Z directions and $\Delta\alpha_{pitch,i}$, $\Delta\alpha_{yaw,i}$, $\Delta\alpha_{roll,i}$ are angular errors for movement in direction *i* across the whole range ΔX, ΔY or ΔZ of the stage. Irrespective of the movement direction, pitch, yaw and roll are defined relative to the X axis.

The vector **D** = [d_x, d_y, d_z] consists of the error components δx_{drift} , meaning drift, and $\delta x_{deadpath}$, meaning dead path error in a laser interferometric measurement, as follows:

(13) $$d_x = \delta x_{drift} + \delta x_{deadpath} + \delta x_{flat} .$$

Similar equations can be written for d_y and d_z. Because errors caused by flatness deviations in the X and Y mirrors and out-of-plane errors in the Z direction (δx_{flat}, δy_{flat} and δz_{oop}) are not corrected but taken as an uncertainty component, they are included in **D**. If corrected, these errors would be coordinate dependent.

The combined standard uncertainties for the coordinates (*x*, *y*, *z*) are: u_{cx}=q[0.48; 0.04*x*; 0.17*y*; 1.7*z*; 2*time*] nm, u_{cy}=q[0.45; 0.31*x*; 0.07*y*; 0.14*z*; 4*time*] nm, and u_{cz}=q[0.42; 3*x*; 7.2*y*; 0.18*z*; 2*time*] nm, where *x*, *y*, *z* are in µm and *time* is in h.

The main uncertainty components are drifts, noise, non-orthogonality of the measurement axes and Abbe errors. In many practical measurements, the effects of drift and noise can be significantly reduced by repetitive measurements and selection of a suitable analysis algorithm. The temperature in the measurement chamber must be stable before performing measurements.

4.4 Calibration of transfer standards

Calibration of pitch and step height standards is one of the main purposes of MAFMs. Calibration of transfer standards is needed to achieve traceability for SPMs and SPM measurements. Uncertainty estimates are needed for both transfer standard calibration and calibration of SPMs.

Different techniques have been developed for calibration of transfer standards. PTB has developed calibration techniques for 1-D [95, 96] and 2-D [97] gratings, and for calibration of step height standards [98]. Uncertainty components in pitch [99] and step height [100] calibration by MAFM have been studied at NMIJ/AIST and by laser diffractometry at NRC [101].

We have developed methods for faster calibration of pitch and step height standards. Faster methods are needed because measurement times with MAFMs are typically longer than with other AFMs.

In pitch calibration, only the sides of the measurement area are measured and the middle area is skipped in order to cut measurement time. The number of measured and skipped periods (n_p) is calculated using pitch value either from an earlier calibration or from a less accurate measurement. Period length is calculated with a 2-D correlation algorithm.

In step height calibration, measurement speed can be adjusted to slow down when approaching an edge. Edge positions are estimated using a previous measurement line. This reduces measurement time and the risk of tip damage.

The measurement model for pitch calibration is

$$p = \frac{l_x(\mathbf{r}_2, \mathbf{r}_1)}{n_p} + P\alpha_t \Delta t_{20°C} + P\left(\frac{\cos\xi_{rotation}}{\cos\xi_{tilt}} - 1\right) + \delta p_{local\ variations} \tag{14}$$

$$\begin{aligned} l_x = {} & c_{xx}(x_{m2} - x_{m1}) + a_{xx}(x_{m2} - x_{m1}) + a_{xy}(y_{m2} - y_{m1}) + a_{xz}(z_{m2} - z_{m1}) \\ & + \delta x_{drift} + \delta x_{deadpath} + \delta x_{flat} + \delta L_{x\ algorithm} \end{aligned}, \tag{15}$$

where $a_{xx}(x_{m2} - x_{m1})$, $a_{xy}(y_{m2} - y_{m1})$, and $a_{xz}(z_{m2} - z_{m1})$ are Abbe errors. Because the analysis is done along the X axis, $y_{m2} = y_{m1}$ and thus the Abbe error related to the Y movement is zero. For the X axis the c_{xx} component is defined to be 1. Cosine errors caused by non-ideal sample alignment (see Figures 14 and 15), i.e. tilt ξ_{tilt} and rotation $\xi_{rotation}$, are corrected. $P\alpha_t\Delta t_{20°C}$ is the correction for thermal expansion, where α_t is the thermal expansion coefficient for the sample and $\Delta t_{20°C}$ is the temperature deviation from 20°C. For simplicity the nominal pitch P is used in the equations for calculation of the correction terms.

The main uncertainty components in the calibration are corrections for sample alignment and the Abbe error in the measurement of the X coordinate.

A simplified model function for step height calibration is:

(16) $$h = \frac{\sum_i^m h_i}{m} + H\alpha_t \Delta t_{20^\circ C} + H\left(\frac{1}{\cos\xi_{tilt}} - 1\right) + \delta h_{local\ variations}$$

(17) $$h_i = \frac{\left(\bar{z}_B - \bar{z}_A\right) + \left(\bar{z}_B - \bar{z}_C\right)}{2}.$$

$\bar{z}_A$, $\bar{z}_B$ and $\bar{z}_C$ are averages of the Z coordinates over areas *A*, *B* and *C*.

(18) $$\bar{z}_A = \frac{\sum_A \left(c_{zz} z_m + a_{zz} z_m + \delta z_{drift} + \delta z_{deadpath} + \delta z_{oop} + \delta x_{Abbe}\right)}{W/2 \cdot \Delta x}$$

and respectively for $\bar{z}_B$ and $\bar{z}_C$. W is the width of the step (see Figure 16) and Δx is the x resolution; i.e. $W/2 \cdot \Delta x$ is number of points in the area. $H\alpha_t \Delta t_{20C}$ is the correction for thermal expansion, where α_t is the thermal expansion coefficient for the sample and $\Delta t_{20^\circ C}$ is the temperature deviation from 20°C. $\cos\xi_{tilt}$ is the correction for the sample tilt (see Figures 14 and 15). The δx_{Abbe} term consists only of the non-linear part of the Abbe correction. For simplicity the nominal step height *H* is used for calculation of the correction terms.

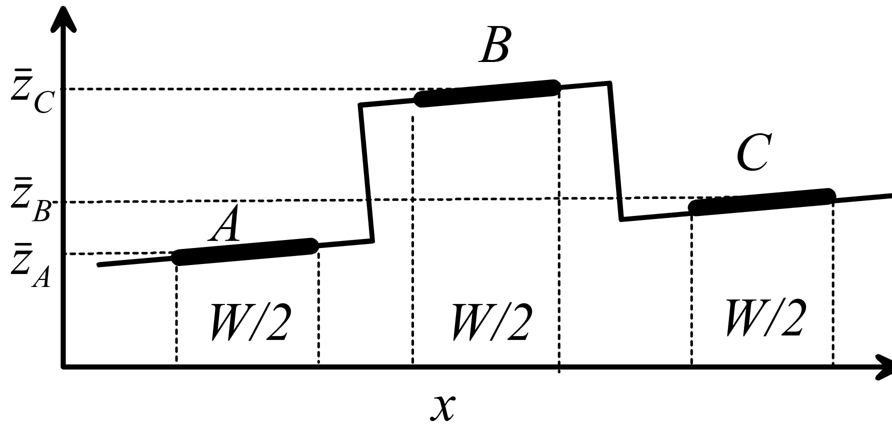

Figure 16 *Areas A, B and C used in step height calibration. W is the width of the step.*

The main uncertainty components are the Abbe error in measurement of the Z coordinate and repeatability of the measurement. Local variations in the step height of the sample were not studied, but in most practical calibrations it could be the largest uncertainty component. To reduce the effect of local variations the measurements should be done in a specified measurement area and should average over the measurement area.

The uncertainty components for both pitch and step height calibrations are analysed in greater detail in paper III.

4.5 Calibration of an AFM

A calibration method for a coordinate system of a commercial AFM PSIA XE-100 AFM was studied in paper IV. The calibration principles set out in 4.2 were followed. The main task was to study the metrological properties of the AFM and calculate realistic uncertainty estimates. Scale calibration methods were studied and as a result, scale errors were corrected by linear correction. Nonlinearity of the scales was included in the uncertainty budget. Abbe errors and orthogonality errors were studied but not corrected for.

In the AFM, the Z movements are mechanically separated from the X and Y movements. The XY stage with optical position sensors and closed loop control moves the sample in the X and Y directions under the AFM head. X and Y translators under the XY stage are used for positioning the sample. A separate piezo stage, also with a position sensor, moves the AFM tip in the Z direction. The structure of the SPM allows interferometric calibration of all three measurement axes.

A simplified model function for a measurement point **r** = [*x, y, z*] of the coordinate system is:

$$
\begin{aligned}
x &= C_x(x_m, s_{rate}, s_{range})\, x_m + \delta z \sin\left(\delta\alpha_{pitch,x}(x,y)\right) \\
&\quad + \delta y \sin\left(\delta\alpha_{yaw}(x,y)\right) + z_m \sin\left(\gamma_{xz} - 90^0\right) + \delta x_{drift} \\
y &= C_y(y_m, s_{rate}, s_{range})\, y_m + \delta z \sin\left(\delta\alpha_{roll,x}(x,y)\right) \\
&\quad + \delta x \sin\left(\delta\alpha_{yaw}(x,y)\right) + x_m \sin\left(\gamma_{xy} - 90^0\right) + z_m \sin\left(\gamma_{yz} - 90^0\right) + \delta y_{drift} \\
z &= C_z(z_m) z_m + \delta z_{oop}(x,y) + \delta z_{drift}
\end{aligned}
\quad , \qquad (19)
$$

where C_X, C_y, and C_Z are scale correction functions for the X, Y and Z scales. The scale corrections are functions of the measured *x, y* and *z* co-ordinates **m** = [x_m, y_m, z_m] and they could also be functions of the scan rate (s_{rate}) and the total scan range (s_{range}). δx, δy and δz are Abbe offsets in the X, Y and Z directions. $\delta\alpha$s are angular errors and γs are angles between the *x*, *y* or *z* axes (i.e. γ - 90° are orthogonality errors). For simplicity we assume that the coordinate system X axis is parallel to the measured *x* coordinates. $\delta z_{oop}(x,y)$ is a correction for out-of-plane deviation. δx_{drift}, δy_{drift} and δz_{drift} are drift corrections. The model function (19) is used to calculate uncertainty estimates for the coordinate system.

The scales were calibrated by two different methods: laser interferometer and calibrated pitch standard. Laser interferometric calibration allows both the measurement of unlimited measurement points and for more versatile calibration structures, thus enabling

the study of linearity behaviour. The scale corrections measured by interferometers and gratings are slightly different, probably due to the effects of the scan range, turning point errors and Abbe errors. These results indicated some misalignment in the XY scanner, which was sent for repair. Measurements after the repair showed that the scale correction does not depend on the scan range and the default overscan (10% - 15%) is sufficient at least for measurement ranges larger than ± 1 μm.

The scale corrections used in this study include only linear corrections. The given uncertainty includes only the uncertainty that arises from non-linearity of the scale. Other uncertainty components have to be included case-specifically.

The Z detector scale was calibrated by a laser interferometer. Design of the AFM allows interferometric calibration during a real AFM measurement. The XY scanner was removed and replaced by a plane mirror laser interferometer and a piezo actuator. The mirror was moved step-by-step in the Z direction and the position was measured simultaneously by both the interferometer and the AFM. The measurement setup would allow various stepping structures, but simple up-down-up-down stepping was used. This mimicked the measurements of a step height standard.

The structure of our AFM requires that special attention be paid to the minimization of Abbe offsets. Because of the separate XY stage and Z stage and sample positioning by the translators under the XY scanner stage, in the worst case the Abbe offset in all directions might be as much as a few centimetres. The Abbe offset can be minimized if the thicknesses of the calibration grid and measured sample are the same and they are measured at the same position of the XY scanner. We have minimized the Abbe offset by adding small translators on top of the XY scanner. Thus, the calibration and measurement can be done in the same scanner position and the upper translator can be used for the sample alignment.

Angular errors were measured by a position sensitive detector (PSD) and a laser beam. The stage was driven parallel to the measurement beam, and the position of the laser beam reflected back simultaneously from a mirror mounted on the scanner stage was recorded by the PSD. Yaw and pitch angles of the movement were calculated from position deviations at the PSD.

Orthogonality of the axes was measured using calibration standards and an error separation method. A 2-D grating was used in measurement of the orthogonality of the X and Y axes and a triangular grating for the Z axis.

The out-of-plane error, i.e. the flatness error of the AFM, was measured using a flatness standard. The data was flattened by a first order average profile fit and averaged over the slow scan direction. The observed out-of-plane deviation of the X axis was small, but slightly larger for the Y axis. The effect of the out-of-plane error in measurements can be minimized using the X axis as a fast scanning axis. In a slow scan direction, the effect of drifts is usually larger than the out-of-plane error, and the drift is corrected by first, second or third order plane correction.

Errors or uncertainties due to drifts were not studied in paper IV. The effects of drifts are case-specific and the effects should be considered individually for each measurement, depending on the measured sample, measurement time, measurement range, temperature variations, setting time etc. The effect of drifts could be studied using the same method

used in the characterization of the IT-MAFM in paper II. Dynamic errors in the movements may be significant. The best results will be reached if calibration is done with the same scanning range and scanning rate as the measurements. The IT-MAFM or substitution method will be used in the most accurate measurements.

4.6 Results

International comparisons between NMIs are a way to guarantee the reliability of their measurements. MIKES has participated in two comparisons related to the results of this thesis: the Euramet 925 comparison for 1-D gratings and step height standards, and the CCL-Nano5 comparison for 2-D gratings. The MIKES IT-MAFM was used in the former and the calibrated AFM in the latter. In the Euramet 925 comparison the samples were nominally 300 nm and 700 nm pitch and 7 nm, 40 nm, 1000 nm and 2000 nm step height standards. Standard uncertainties for MIKES measurements were 0.022 nm and 0.034 nm for pitch and 0.35 nm – 0.64 nm for step height measurements. In the CCL-Nano5 comparison the samples were 2-D gratings with pitch of 300 nm and 1000 nm, and nominal angle of 90°. The MIKES results were in good agreement with the reference values in both comparisons. The results for 300 nm pitch and 7 nm step height are shown in Figures 17-19.

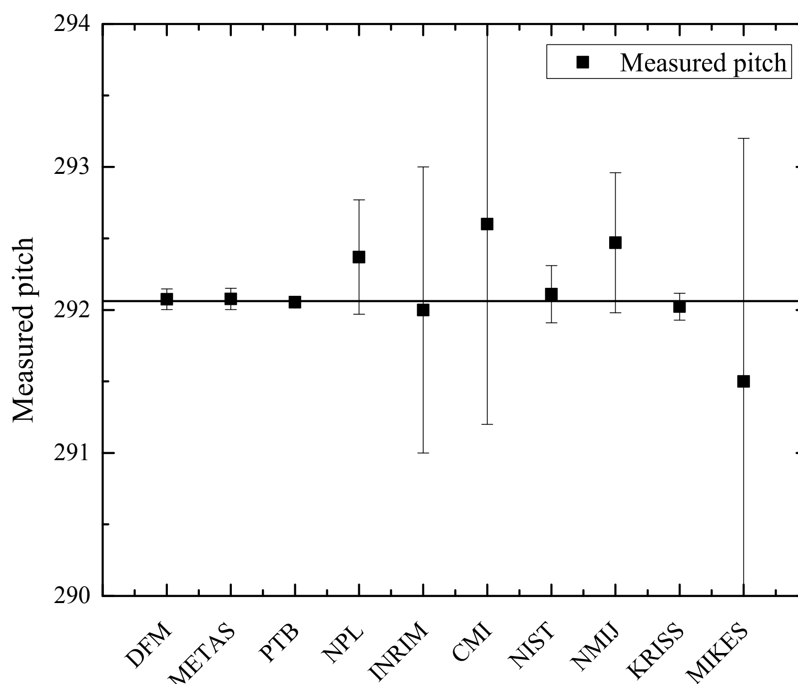

Figure 17 *Pitch measured with SPM by participating NMIs in the CCL-Nano5 comparison. The straight line is the reference value and uncertainties are standard uncertainties. The reference value includes results measured with optical diffraction, but they are not shown here.*

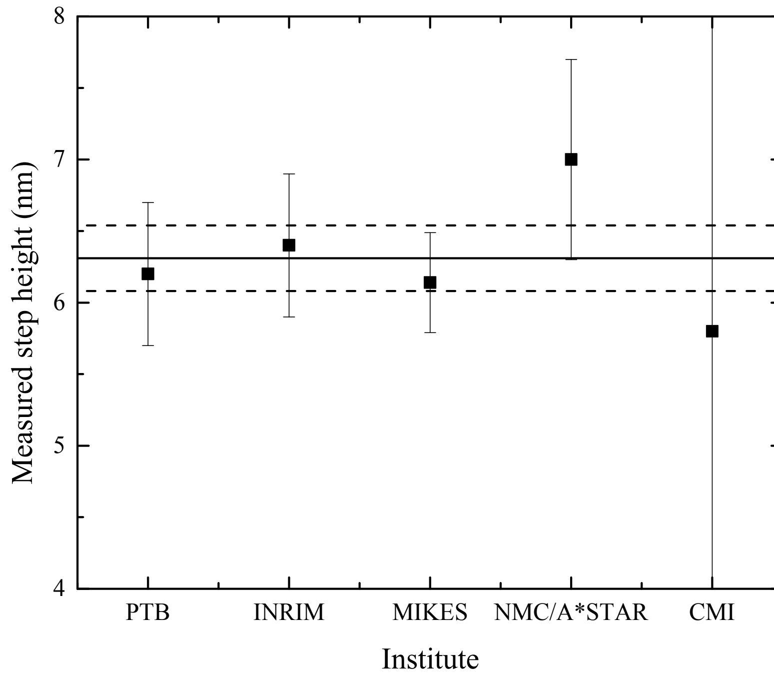

Figure 18 *Step height measured with SPM by participating NMIs in the Euramet 925 comparison. The straight line is the reference value and dashed lines are the standard uncertainty of the reference value. Standard uncertainties of the measurements are shown.*

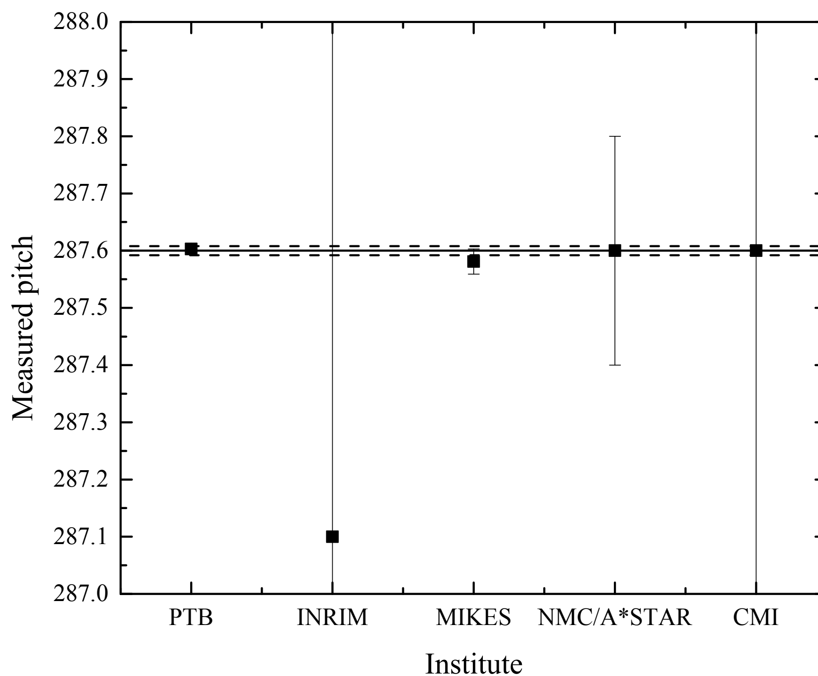

Figure 19 *Pitch measured with SPM by participating NMIs in the Euramet 925 comparison. The straight line is the reference value and dashed lines are the standard uncertainty of the reference value. Standard uncertainties of the measurements are shown.*

5 Laser diffractometer

Laser diffractometry is a simple and fast but accurate method for measurement of grating pitch. MIKES has therefore developed a laser diffractometer as an alternative traceability route for calibration of 1-D and 2-D gratings. The laser diffractometer is also used in the validation of the IT-MAFM.

5.1 Principle of laser diffraction

The principle of the laser diffraction measurement is quite simple. The laser diffractometer developed in this thesis is based on the Littrow configuration. The Littrow condition is satisfied when the laser beam diffracts back to the direction of the incident beam. The pitch of the grating p_m can be calculated from the mth order diffraction angle θ_m by

$$p_m = \frac{m\lambda_0}{2n\sin\theta_m} , \qquad (20)$$

where λ_0 is the vacuum wavelength of the light source and n is the refractive index of air. The Littrow configuration diffractometer is both optically and theoretically simple and the configuration is used in several other diffractometers at METAS (Switzerland) [102], NRC (Canada) [103], the Japan Quality Assurance Organization (JQA), [104], and CMS/ITRI (Taiwan) [105]. There are also other types of diffactometers, such as the PTB (Germany) design based on a slightly off-Littrow configuration [106],the KRISS (Korea) design based on a conventional diffraction method [107], or the laser interference diffractometry method BIPM/VNIIM (Russia) [108]. Diffractometers have been developed by several NMIs (see table 2).

Table 2. *Laser diffractometers developed by different NMIs and examples of uncertainty estimates for pitch p = 300 nm measurement. Uncertainties reported in comparisons are given if they are smaller than uncertainties in CMC.*

Country	NMI	Standard uncertainty	Ref
Finland	MIKES	0.0013 0.026 nm*	I
Switzerland	METAS	0.0075 nm* 0.0031 nm***	102
Canada	NRC	0.0035 nm	103
Czech Republic	CMI	0.039 nm* 0.041***	
Germany	PTB	0.010 nm*	106

		0.0032 nm**	
Japan	JQA	0.085 nm ***	104
Korea	KRISS	0.0067 nm*	107
		0.0020 nm**	
		0.006 nm***	
Taiwan	CMS/ITRI	0.0045 nm*	
		0.003 nm***	
Italy	INRIM	0.0075 nm*	
		0.005 nm**	
United Kingdom	NPL	0.031 nm*	
		0.0043 nm***	
Russia	VNIIM	0.2 nm**	108
China	NIM	0.0015**	

* CMC database
** CCL-Nano4 comparison [5]
*** CCL-Nano5 comparison [6]

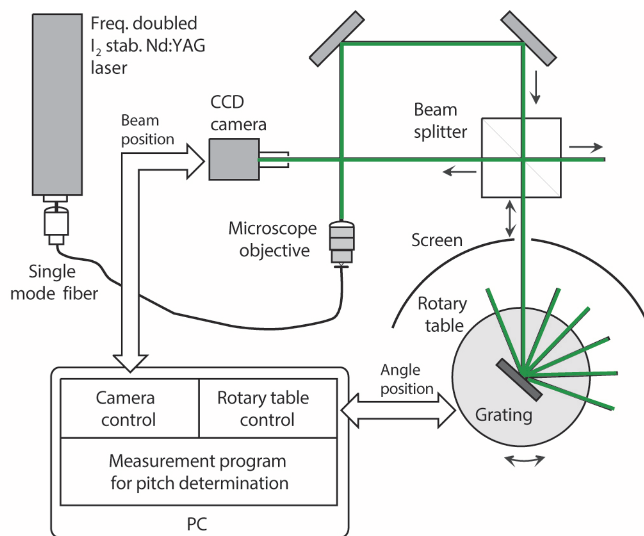

Figure 20 *Laser diffraction setup* [I]

5.2 Measurement setup

The measurement setup is shown in Figure 20. The setup consists of a frequency doubled iodine stabilized Nd:YAG laser fibre-coupled to the setup. A rotary table is used to rotate the grating to fulfil the Littrow condition. A beam splitter is used to direct the diffracted beam to the CCD, which is used to detect the position of the diffracted beam. In addition,

there are mechanics for the sample alignment and a screen to help coarse alignment. The beam is collimated using a microscope objective and aligned by two mirrors.

The CCD camera is used as a null detector to detect when the Littrow condition is fulfilled. The Littrow position on the CCD is predefined during the alignment of the system. Use of a CCD allows measurement of the diffraction angle around the Littrow position, and these angles can be used to compensate for small periodical nonlinearity of the angle scale. Another advantage of using a CCD instead of other position sensitive or line detectors is that the shape of the diffracted beam can be seen. In addition, the CCD allows fast and easy alignment of the sample.

The pitch p is calculated as a weighted average of the pitches calculated from different diffraction orders p_m, see (20). The diffraction angle is defined as half of the angle between $+m^{th}$ and $-m^{th}$ order diffractions. This eliminates the problem of defining the 0th order diffraction.

$$p = \frac{\sum w_m \cdot p_m}{\sum w_m} \qquad (21)$$

where the weights w_m are defined as

$$w_m = \frac{1}{\left(\frac{\partial p}{\partial \theta_m} \cdot u_c(\theta_m)\right)^2} = \left(\frac{\tan\theta_m}{P \cdot u_c(\theta_m)}\right)^2, \qquad (22)$$

where $u_c(\theta_m)$ is the standard uncertainty of the θ_m measurement. For simplicity p_m can be replaced by the nominal pitch P in the evaluation of the sensitivity coefficient $\partial p/\partial\theta_m$ with negligible error.

5.3 Traceability and uncertainty of the diffractometer measurement

The traceability of the laser diffraction measurement to the SI comes via the vacuum wavelength of the laser and the angle scale. An iodine stabilized Nd:YAG laser is used in the setup. The laser is also used in the realization of the metre, i.e. it provides a very accurate and traceable vacuum wavelength. The refractive index of air is determined using the Edlén formula [19] and traceably measured pressure, temperature and humidity. Traceability to the angle scale comes via the developed calibration method based on error separation (see chapter 5.3.1).

A weighted average is used in the calculation of pitch, because sensitivity coefficients depend on the diffraction angle θ_m, i.e. for diffraction angles having larger m the sensitivity coefficient and, thus, the uncertainty of the pitch becomes smaller (see uncertainty bars in Figure 22). The model function for the pitch p calculated as a weighted average of p_m

$$p = \left[1 + \alpha_t \Delta t_{20^\circ C}\right] \frac{\cos\Omega}{\cos\tau} \frac{\lambda_0}{2n} \frac{\sum_m p_m w_m}{\sum_m w_m}, \tag{23}$$

where α_t is the coefficient of the thermal expansion of the sample, Δt_{20C} is the temperature deviation from 20C, w_m is the weight, Ω is the grating roll and τ is the beam tilt. The errors due to the sample roll and the beam tilt are cosine type errors. The measured pitch is a projection of the real pitch to the X axis, which causes the cos Ω term. The beam tilt causes a $(\cos\tau)^{-1}$ type error, since only the projection of the wave vector is measured in the Littrow configuration.

The main uncertainty source in the measurement is the diffraction angle measurement, i.e. the angle scale and the determination of the centroid of the beam. A fibre coupled laser beam is used to get a good quality beam. Uncertainty components caused by the alignment of the sample and the laser beam can be reduced to a negligible level by careful alignment. It is assumed that the beam size is smaller than the grating size with all measured diffraction orders, in which case the distance between the sample surface and the rotation axis does not affect the pitch [102], otherwise it should be taken into account as an uncertainty component [109]. Because of the temperature-controlled laboratory environment, temperature effects on the measurement are small.

5.3.1 Traceability of the angle scale

A new way to realize the radian using the error separation method with an uncalibrated grating and a rotary table is developed in paper IV. In the laser diffraction setup a grating is mounted on a rotary table and the diffraction angles are measured in the Littrow configuration. The measurement of the diffraction pattern is repeated in different orientations of the rotary table. A calibration correction table for the rotary table is calculated from the data. A novel fitting algorithm is used to separate the angle scale error in the rotary table and in the grating pitch.

The angle error of the rotary table was measured with the new self-calibration method and the results were compared with the results measured using an autocollimator and calibrated 12-face polygon (see Figure 21). Small details of the error curve cannot be detected in the polygon calibration, because number of measurement points is limited by the polygon. In the self-calibration method, more measurement points can easily be measured (in our case 320 points). The standard uncertainty of the angle calibration was

0.92″. The properties of the rotary table limit the reached uncertainty, not the calibration method. Thus, better accuracy could be achieved with a more stable rotary table.

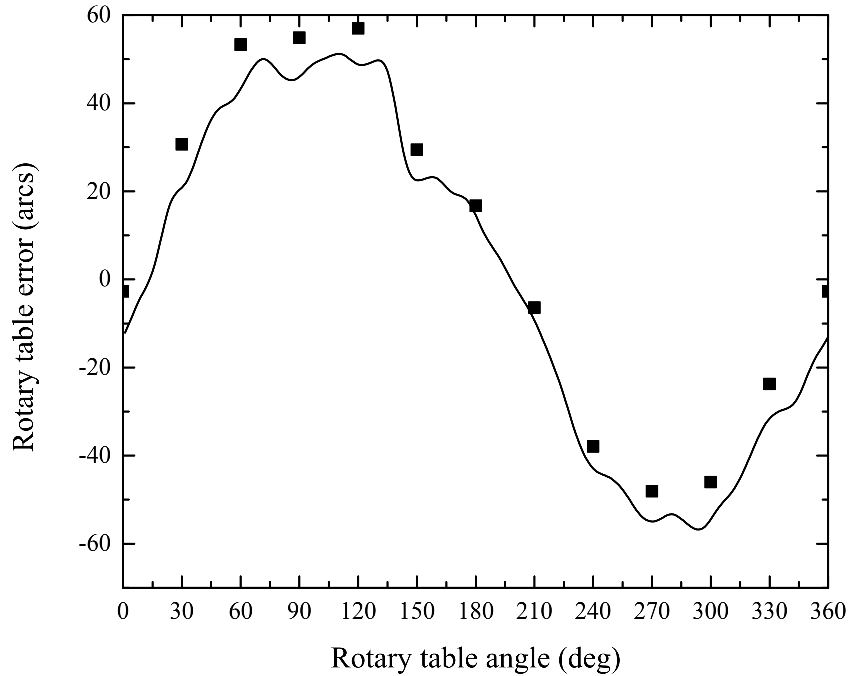

Figure 21 *Rotary table angle error measured with the self-calibration method (solid line) and with an autocollimator and 12-face polygon (squares).*

5.4 Results

Three gratings with different nominal pitch (2 µm, 700 nm and 300 nm) were measured using laser diffraction.

The measurement results for 2 µm pitch are shown in Figure 22 for diffraction orders $m = 1...6$. The same measurement was repeated in different sample holder orientations related to the angle encoder scale. Differences in these measurements are mainly caused by calibration of the angle scale. The measurement was also repeated so that the sample was removed from the holder and realigned before each measurement. The differences in these measurements are caused by different alignments.

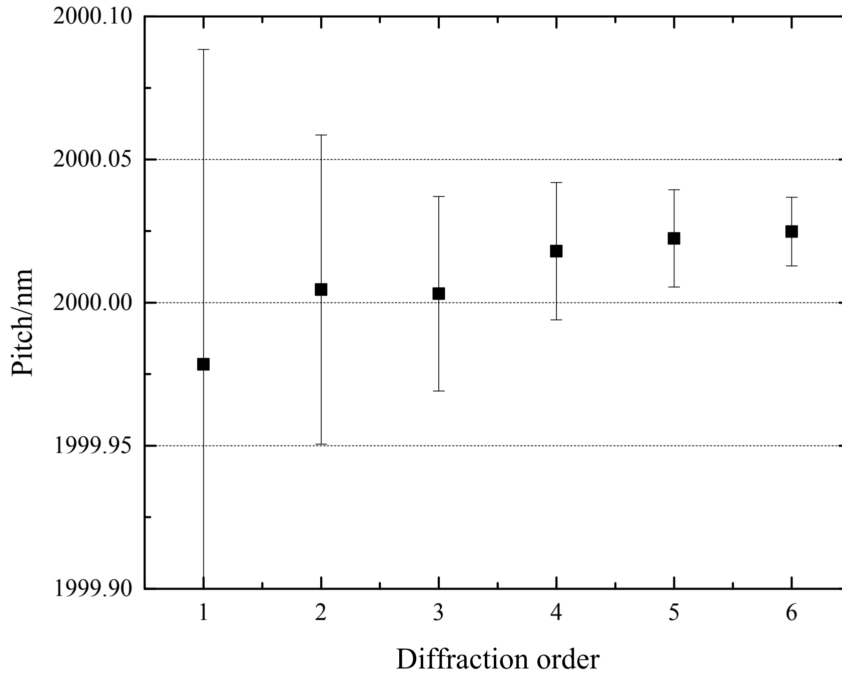

Figure 22 *Measured pitch values with standard uncertainties for different orders. The bars indicate the standard uncertainty of the pitch for particular diffraction order.*

The laser diffraction measurements were compared against the MIKES IT-MAFM. Gratings with a nominal pitch of 300 nm and 700 nm were measured with both the diffractometer and the IT-MAFM. The results are shown in Table 3. The results are in good agreement with each other. Differences between the diffractometer and IT-MAFM measurements are 6 pm and 45 pm for 300 nm and 700 nm nominal pitch, respectively.

Table 3. *Pitches measured with both a diffractometer and IT-MAFM.*

Nominal pitch/nm	Diffractometer /nm	u_c/pm	IT-MAFM/nm	u_c/pm
300	287.575	1.3	287.581	22
700	700.757	4.4	700.712	34

6 Discussion

The need for traceable measurements at nanometre scale are expected to increase in the near future. Commercialization of nanotechnology and mass production need reliable measurements. Traceable measurements are needed also for legislation, industrial safety and estimation of environmental effects.

Nanometrology will be one of the focuses of metrology also in the future. Four core applications for nanometrology are listed in the micro- and nanometrological roadmap: nanoparticles, functionalized surfaces, semiconductor & nano-electronics, and nanobiotechnology [3]. The research done in this thesis completes the traceability chain for fairly simple dimensional nanoscale measurements. The next step is the development of traceable measurement methods for more complex structures and material properties as mentioned in the roadmap. At MIKES we have developed measurement methods for nanoparticles in co-operation with other NMIs [110]. We are also participating in several on-going EU funded EMRP (European metrology research project) nanometrology projects. As part of the MecProNO project we shall be developing measurement methods for mechanical properties of nano-objects [11]. The CRYSTAL project is looking at different crystalline and self-assembly structures as possible materials for calibration standards [14]. In the future, a calibration method will be developed for critical dimension, e.g. line width, measurements.

The laser diffractometer has been developed further for angular scatterometric measurements as part of the SCATTERO project [111], which is planning reliable measurement methods for diffractive optics elements and the semiconductor industry.

The correction method for the nonlinearity of the laser interferometer has been developed further for picometre level measurements [51, 52].

The IT-MAFM is part of the traceability chain for stylus instruments and thus for surface roughness measurements [112]. We have started a calibration service for grating pitch and step height standards.

MIKES has organized the Nordic-nano1 comparison for research institutes and universities in Finland, Sweden, Norway and Estonia in co-operation with the NMIs in these countries. There were 26 participants, some of which reported more than one instrument. The comparison samples were nominally 300 nm and 700 nm. The results for 300 nm samples are shown in Figure 23. The error bars show uncertainty estimates given by the participants, but they are not always standard uncertainties. The results of the comparison show that calibration of the instruments would increase the accuracy significantly for many laboratories. [113] In 2014 we plan to launch the Nordic-nano2 comparison for step height measurements.

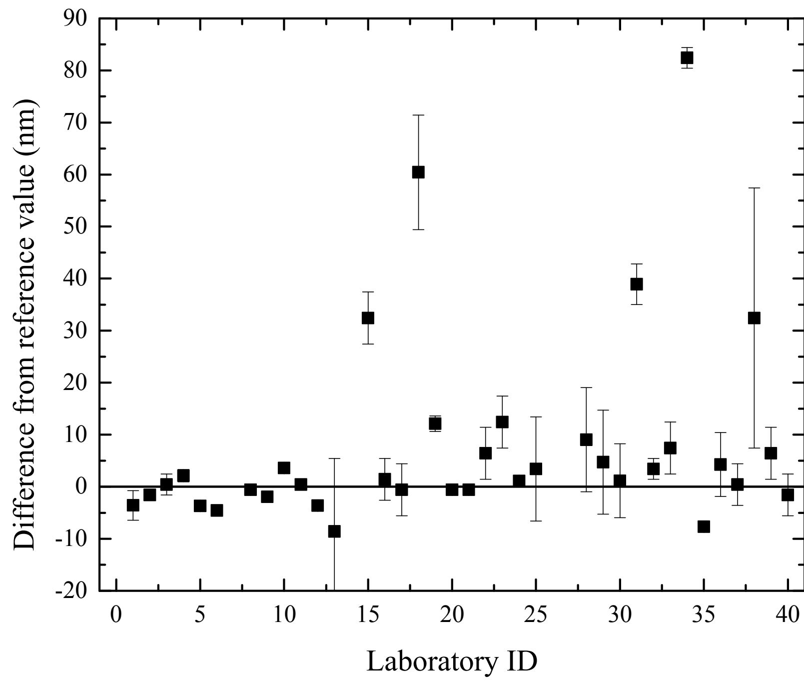

Figure 23 *Differences from the reference value for nominally 300 nm pitch standard in the Nordic-nano1 comparison.*

7 Conclusions

In this thesis the traceability chain for nanometre scale measurements in Finland was established. This includes calibration services for calibration standards for modern microscopes. The results of this thesis form the basis for further studies in nanometrology at MIKES.

An interferometrically traceable metrological atomic force microscope [II] and laser diffractometer [I] with direct traceability to the definition of the metre were developed. In addition, calibration methods for transfer standards [III] and commercial AFMs [IV] were established.

Nanometre scale measurements require new, more accurate measurement methods. Therefore, a new method for correction of interferometer nonlinearity was developed [II]. Measurement of refractive index is crucial in accurate interferometric measurements, thus we developed a new method for determination of the refractive index of air along the interferometer beam path [V].

In pitch measurement using a laser diffractometer, the main error component is uncertainty of the diffraction angle measurement. Therefore, a new calibration method for the angle scale of a rotary table was developed [I]. The method can be used as a realization of the angle scale.

Uncertainty estimates are a crucial part of traceability. Therefore, careful uncertainty analysis was included in all the studies of this thesis [I-V].

References

[1] BIPM. “International Vocabulary of Metrology – Basic and General Concepts and Associated Terms”, JCGM 200:2012

[2] CCL-WGDM7, 1998, revised in 2003. Conclusions of the WGDM 3 Discussion Group on Nanometrology, 25 June, 1998

[3] TC-Length EURAMET TC-L roadmap: “Micro&Nano” 29 July 2012

[4] Danzebrink, H-U, Koenders L, Picotto GB, Lassila A, Wang SH and Klapetek P, “Final report on EUROMET.L-S15.a (EUROMET Project 925): Intercomparison on step height standards and 1D gratings.” *Metrologia*, 47, Tech. Suppl., 04006 (2010)

[5] Meli F, “NANO4-1D Gratings, Final report.” (2000)

[6] Garnaes J, Dirscherl K. “NANO5—2D Grating—Final report CCL-S4.” *Metrologia, Tech. Suppl.,* 45, 04003 (2008)

[7] Koenders L, Bergmans R, Garnaes J, Haycocks J, Korolev N, Kurosawa T, Meli F, Park BC, Peng G-S, Picotto GB, Prieto E, Gao S, Smereczynska B, Vorburger T and Wilkening G, “Comparison on Nanometrology: Nano 2—Step height.” *Metrologia* **40** 04001 (2003)

[8] Koenders L, Klapetek P, Meli F and Picotto GB, “Comparison on step height measurements in the nano and micrometre range by scanning force microscopes.” *Metrologia* **43** 04001 (2006)

[9] http://projects.npl.co.uk/metnems/index.html

[10] Seppä J, Kassamakov I, Heikkinen V, Nolvi A, Paulin T, Lassila A and Hæggsröm E, “Quasidynamic calibration of stroboscopic scanning white light interferometer.” *Optical Engineering*, **52**(12), pp.124104, (2013)

[11] http://www.ptb.de/emrp/mechprono-home.html

[12] Bodermann B, Hansen PE, Burger S, Henn MA, Gross H, Bär M, ... and Wurm M, “First steps towards a scatterometry reference standard.” In *SPIE NanoScience+ Engineering* (pp. 84660E-84660E). International Society for Optics and Photonics. (2012, October).

[13] http://www.ptb.de/emrp/subnano-home.html

[14] http://www.ptb.de/emrp/sib61-home.html

[15] BIPM, IEC, IFCC, ISO, IUPAC, IUPAP and OIML, “Guide to the expression of uncertainty in measurements.” JCGM 100:2008

[16] Reeve C, “The calibration of indexing tables by subdivision.” *NBS Internal Report* 75-750, (1975)

[17] Cook AH, “The calibration of circular scales and precision polygon.” *British Journal of Applied Physics,* **5,** 367-371 (1954)

[18] Edlén B, “The Refractive Index of Air.” *Metrologia*, **2**, 71-80 (1966).

[19] Bönsch G and Potulski E, “Measurement of the refractive index of air and comparison with modified Edlen's formula” *Metrologia*, **35**, 133-139 (1998).

[20] Birch KP and Downs MJ, “An Updated Edlén Equation for the Refractive index of Air.” *Metrologia*, **30**, 155-162 (1993).

[21] Birch KP and Downs MJ, “Correction to the Updated Edlén Equation for the Refractive index of Air.” *Metrologia*, **31**, 315-316 (1994).

[22] Korpelainen V, Hemming B, Lehto H and Lassila A, “A New Acoustic Method for Determination of the Effective Air Temperature for Length Interferometers.” in *Proc of the euspen Int. Topical Conference*, Aachen, Germany, May 19th/20th, 431-434 (2003).

[23] Hieta T and Merimaa M, "Spectroscopic measurement of air temperature." *International Journal of Thermophysics* 31.8-9, 1710-1718 (2010).

[24] Hieta T, Merimaa M, Vainio M, Seppä J and Lassila A, “High-precision diode-laser-based temperature measurement for air refractive index compensation.” *Applied Optics*, *50*(31), 5990-5998 (2011).

[25] Earnshaw KB and Owens JC, “Dual wavelength optical distance measuring instrument, which corrects for air density.” *IEEEJ. Quantum Electron*, **3**, 544-550 (1967).

[26] Matsumoto H and Honda T, “High-accuracy length-measuring interferometer using the two-colour method of compensating for the refractive index of air.” *Meas. Sci. Technol*., **3**, 1084-1086 (1992).

[27] Meiners-Hagen K and Abou-Zeid A, “Refractive index determination in length measurement by two-colour interferometry.” *Meas. Sci. Technol.,* **19,** 084004 (2008).

[28] Renkens MJ and Schellekens PH, “An Accurate Interference Refractometer Based on a Permanent Vacuum Chamber – Development and Results” *Annals of the CIRP*, **41**, 581-583 (1993).

[29] Tianchu Li, “Design principles for laser interference refractometers.” *Measurement*, **16**, 171-176 (1995).

[30] Downs MJ and Birch KP, “Bi-directional fringe counting interference refractometer.” *Precision Engineering*, **5**, 105-110 (1983).

[31] Lassila A, Korpelainen V and Mihaljov L, “Refractive index of air compensation by acoustic method for plane mirror interferometer.” *Proceedings of NanoScale 2006*, 24 – 25 April, Bern, Switzerland,

[32] Cramer O, “The variation of the specific heat ratio and the speed of sound in air with temperature, pressure, humidity, and CO_2 concentration.” *J. Acoust. Soc. Am.,* **93** (5), 2510-2516 (1993).

[33] Morfey CL and Howell GP, “Speed of sound in air as a function of frequency and humidity.” *J. Acoust. Soc. Am*., **68**, 1525-1527 (1980).

[34] Howell GP and Morfey CL, “Frequency dependence of speed of sound in air.” *J. Acoust. Soc. Am.*, **82**, 375-377 (1987).

[35] Quenelle RC. “Nonlinearity in Interferometric measurements.” *Hewlett-Packard Journal*, April 1983, p 10 (1983).

[36] Bobroff N, “Recent advances in displacement measuring interferometry.” *Meas. Sci. Technol*. **4**, 907-26 (1993).

[37] Wu C, Lawall J and Deslattes D, “Heterodyne interferometer with subatomic periodic nonlinearity.” *Appl. Opt*., **38**, 4089–94 (1999).

[38] Cosijns SJAG, Haitjema H and Schellekens PHJ, ”Modelling and verifying non-linearities in heterodyne displacement interferometry.” *Prec. Eng.,* **26**, 448-455 (2002).

[39] Schmitz TL, Chu DC and Kim HS, “First and second order periodic error measurement for non-constant velocity motions.” *Prec. Eng.*, **33**, 353-361 (2009).

[40] Eom TB, Choi TY, Lee KH, Choi HS and Lee SK, “A simple method for the compensation of the nonlinearity in the heterodyne interferometer.” *Meas. Sci. Technol*., **13**, 222-225 (2002).

[41] Downs MJ and Nunn JW, “Verification of the sub-nanometric capability of an NPL differential plane mirror interferometer with a capacitance probe.” *Meas. Sci. Technol*., **9**, 1437-1440 (1998).

[42] Yacoot A and Downs MJ, “The use of x-ray interferometry to investigate the linearity of the NPL Differential Plane Mirror Optical Interferometer.” *Meas. Sci. Technol.,* **11**, 1126–1130 (2000).

[43] Hou W and Zhao X, “Drift of nonlinearity in the heterodyne interferometer.” *Prec. Eng.,* **16**, 25-35 (1994).

[44] Pisani M, “A homodyne Michelson interferometer with sub-picometer resolution.” *Meas. Sci. Technol.,* **20**, 084008 (6pp) (2009).

[45] Hou W, “Optical parts and the nonlinearity in heterodyne interferometers.” *Prec. Eng.,* **30**, 337-346 (2005).

[46] Heydemann PLM “Determination and correction of quadrature fringe measurement error in interferometers.” *Appl. Opt*., **20**, 3382-2284 (1981).

[47] Birch K, “Optical fringe subdivision with nanometre accuracy.” *Prec. Eng*., **12**, 195-198 (1990).

[48] Korpelainen V and Lassila A, “Self-calibration of non-linearities of laser interferometer and capacitive sensor combination for an interferometrically traceable AFM device.” *Proc. EUSPEN* (Glasgow, UK, 31 May–2 June 2004) p 256 (2004).

[49] Wu C, “Periodic nonlinearity resulting from ghost reflections in heterodyne interferometry.” *Opt. Comm.,* 215 17-23 (2003).

[50] Kren P and Balling P, “Common path two-wavelength homodyne counting interferometer development.” *Meas. Sci. Technol.,* **20**, 084009 (4pp) (2009).

[51] Seppä J, Korpelainen V, Merimaa M, Picotto GB and Lassila A, “A method for linearization of a laser interferometer down to the picometre level with a capacitive sensor.” *Meas. Sci. Technol.,* **22**, 094027 (2011).

[52] Pisani M, Yacoot A, Balling P, Bancone N, Birlikseven C, Çelik M, Flügge J, Hamid R, Köchert P, Kren P, Kuetgens U, Lassila A, Picotto GB, Şahin E, Seppä SJ, Tedaldi M and Weichert C, “Comparison of the performance of the next generation of optical interferometers.” *Metrologia,* **49**, 455, doi:10.1088/0026-1394/49/4/455 (2012).

[53] Binnig G, Rohrer H, Gerber Ch and Weibel E, “Surface Studies by Scanning Tunneling Microscopy” *Phys. Rev. Lett*., **49**, p 57 (1982).

[54] Binnig G, Quate CF and Geber Ch, “Atomic ForceMicroscope.” *Phys. Rev. Lett.*, **56**, No. 9, p 930 (1986).

[55] VDI/VDE 2656 Part 1: Determination of geometrical quantities using Scanning Probe Microscopes - Calibration of measurement systems.

[56] Dziomba T, Koenders L and Wilkening G, “Towards a Guideline for SPM Calibration Nanoscale Calibration Standards and Methods.” *Dimensional and Related Measurements in the Micro- and Nanometer range*. Edited by G Wilkening and L Koenders (New York: WILEY-VCH GmbH & Co.), pp 173-192 (2005).

[57] Dorozhovets N, Hausotte T, Manske E, Jager G and Hofmann N, “Metrological scanning probe microscope.” *Proc. SPIE Vol. 6188*, 155-162. (2006).

[58] Dorozhovets N, Hausotte T, Hofmann N, Manske E and Jäger G, “Development of the interferometrical scanning probe microscope.” *Interferometry XIII: applications.* San Diego, Calif. (2006).

[59] Dorozhovets N, Hausotte T, Manske E and Jäger G, “Novel investigations and developments in a metrological scanning probe microscope.” *Proceedings of ICPM,* 61-62, Ilmenau, Germany (2008).

[60] Bienias M, Gao S, Hasche K, Seemann R and Thiele K, “A metrological scanning force microscope used for coating thickness and other topographical measurements.” *Appl. Phys*. A, **66**, 837-842 (1998).

[61] Dai G, Pohlenz F, Danzebrink HU, Hasche K and Wilkening G, “Improving the performance of interferometers in metrological scanning probe microscopes.” *Meas. Sci. Technol*., **15**, 444-450 (2004).

[62] Dai G, Pohlenz F, Min X, Koenders L, Danzebrink H-U, Xu M, Hasche K and Wilkening G, “Metrological large range scanning probe microscope.” *Rev. Sci Instr.*, **75**, 962-969 (2004).

[63] Gonda S, Doi T, Kurosava T, Tanimura Y, Hisata N, Yamagishi T, Fujimoto H and Yukawa H, "Real-time interferometrically measuring atomic force microscope for direct calibration of standards." *Rev. Sci. Instr.*, **70**, 3362-3368 (1999).

[64] Misumi I, Gonda S, Huang Q, Keem T, Kurosawa T, Fujii A, Hisata N, Yamagishi T, Fujimoto H, Enjoji K, Aya S and Sumitani H, "Sub-hundred nanometre pitch measurement using an AFM with differential laser interferometers for designing usable lateral scales." *Meas. Sci. Technol.,* **16**, 2080-2090 (2005).

[65] Teague EC, "The National Institute of Standards and Technology molecular measuring machine project: metrology and precision engineering design." *J. Vac. Sci. Technol.,* **B 7**, 1898-1902 (1989)

[66] Kramar JA, "Namometre resolution metrology with the Molecular Measuring Machine." *Meas. Sci. Technol*., **16**, 2121-2128 (2005).

[67] Schneir J, McWaid TH, Alexander J and Wilfley BP, "Design of an atomic force microscope with interferometric position control." *J. Vac. Sci. Technol.,* **B 12**, 3561-3566 (1994).

[68] Dixon R, Köning R, Fu J, Vorburger T and Renegar B, "Accurate dimensional metrology with atomic force microscopy." *Proc. SPIE* 3998, 362-368 (2000).

[69] Meli F and Thalmann R, "Long-range AFM profiler used for accurate pitch measurements." *Meas. Sci. Technol.*, **9**, 1087-1092 (1998).

[70] Haycocks J and Jackson K, "Traceable calibration of transfer standards for scanning probe microscopy." *Prec. Eng*., **29**, 168-175 (2005).

[71] Kim J-A, Kim J-W, Park BC and Eom TB, "Measurement of microscope calibration standards in nanometrology using a metrological atomic force microscope." *Meas. Sci. Technol.,* **17**, 1792-1800 (2006).

[72] Picotto GB and Pisani M, "A sample scanning system with nanometre accuracy for quantitative SPM measurements." *Ultramicroscopy*, **86**, 247-254 (2001).

[73] Lu M, Gao S, Jin Q, Cui J, Du H and Gao H, "An atomic force microscope head designed for nanometrology." *Meas. Sci. Technol.,* **18**, 1735-1739 (2007).

[74] Werner C, Rosielle PCJN and Steinbuch M, "Design of a long stroke translation stage for AFM." *Int. J. Mach. Tool. Manu.*, **50**(2), p183-190 (2010).

[75] Merry RJ, Ronde M J, van de Molengraft R, Koops KR and Steinbuch M, "Directional repetitive control of a metrological AFM." *Control Systems Technology, IEEE Transactions on*, **19**(6), 1622-1629 (2011).

[76] Piot J, Qian J, Kotte G, Van Haesendonck C and Reynaerts D, "Design of a thermally and mecnahically stabile metrological atomic force microscope at KULeuven." *Proc. of the euspen international conference,* San Sebastian, June 2nd -5th 227V2-230V2 (2009).

[77] Piot J, Qian J, Pirée H, Kotte G, Pétry J, Kruth JP and Reynaerts D, "Design of a sample approach mechanism for a metrological atomic force microscope." *Measurement*, **46**(1), 739-746 (2013).

[78] Ducourtieux S, Poyet B and David J, "Development of a metrological atomic force microscope with minimized Abbe error and differential interferometer based real-time position control." *Meas. Sci. Technol.,* **22**, 094010 (15pp) (2011).

[79] Boukellal Y, Ducourtieux S and Poyet B, "Improvement of the LNE's metrological Atomic Force Microscope (mAFM) performance: Design of new mAFM head dedicated for nanometrology applications." In *16th International Congress of Metrology* (p. 06008). EDP Sciences (2013).

[80] Eves BJ, "Design of a large measurement-volume metrological atomic force microscope (AFM)." *Meas. Sci. Technol.,* **20**, 084003 (2009).

[81] Babic B, Freund CH, Herrmann J, Lawn MA and Miles J, "Metrological scanning probe microscope based on a quartz tuning fork detector." *J. Micro/Nanolith. MEMS MOEMS*, **11**(1), 011003 (2012).

[82] Klapetek P, Valtr M and Matula M, “A long-range scanning probe microscope for automotive reflector optical quality inspection.” *Meas. Sci. Technol.,* **22**, 09011 (7pp) (2011).

[83] Vainio M, Merimaa M and Nyholm K, “Optical amplifier for femtosecond frequency comb measurements near 633 nm.” *Appl. Phys*. **B 81**, 1053–7 (2005).

[84] The Scanning Probe Image Processor (SPIP), Image Metrology, Denmark (www.imagemet.com).

[85] www.gwyddion.net

[86] Klapetek P, Nečas D, Campbellová A, Yacoot A and Koenders L, “Methods for determining and processing 3D errors and uncertainties for AFM data analysis.” *Meas. Sci. Technol.*, **22**(2), 025501 (2011).

[87] Garnaes J, Kühle A, Nielsen L and Borsetto F, “True three-dimensional calibration of closed loop scanning probe microscope, Nanoscale Calibration Standards and Methods.” *Dimensional and Related Measurements in the Micro- and Nanometer range.* Edited by G Wilkening and L Koenders (New York: WILEY-VCH GmbH & Co.), pp 193-204 (2005).

[88] Ritter M, Dziomba T, Kranzmann A and Koenders L, “A landmark-based 3D calibration strategy for SPM.” *Meas. Sci. Technol*., **18 S**, 404–414 (2007).

[89] Misumi I, Gonda S, Sato O, Sugawara K, Yoshizaki K, Kurosava T and Takatsuji T, “Nanometric lateral scale development using an atomic force microscope with directly traceable laser interferometers.” *Meas. Sci. Technol.,* **17**, 2041-2047 (2006).

[90] Misumi I, Gonda S, Sato O, Sugawara K, Yoshizaki K, Takatsuji T, Azuma Y, Fujimoto T and Kurosawa T, “Application of GaAs/InGaP superlattice in nanometric lateral scales.” *Meas. Sci. Technol*., **18**, 2743-2749 (2007).

[91] Misumi I, Lu M, Tanaka H, Sugawara K, Gonda S and Kurosava T, “Nanometric lateral scale development with Si/SiO_2 multilayer thin-film structures and improvement of uncertainty evaluation using analysis of variance.” *Meas. Sci. Technol.,* **19**, 045101 (10pp) (2008).

[92] Koenders L, Dziomba T, Thomsen-Schmidt P and Wilkening G, “Standards for the calibration of Instruments for Dimensional Nanometrology.” *Nanoscale Calibration Standards and Methods: Dimensional and Related Measurements in the Micro- and Nanometer range*. Edited by G Wilkening and L Koenders (New York: WILEY-VCH GmbH & Co.), pp 245-258 (2005).

[93] http://nanoscale.de/standards.htm

[94] Abbe E, “Beitrage zur Theorie des Mikroskops und der mikroskopischen Wahrnehmung.” *Archiv Microskopische Anat.,* **9**, 413-463 (1873).

[95] Dai G, Koenders L, Pohlenz F, Dziomba T and Danzebrink H-U, “Accurate and traceable calibration of one-dimensional gratings.” *Meas. Sci. Technol.,* **16**, 1241-1249 (2005).

[96] Chen X and Koenders L, “A novel pitch evaluation of one-dimensional gratings based on a cross-correlation filter.” *Meas. Sci. Technol.,* **25**, 044007 (2014).

[97] Dai G, Pohlenz F, Dziomba T, Xu M, Diener A, Koenders L and Danzebrink H-U, “Accurate and traceable calibration of two-dimensional gratings.” *Meas. Sci. Technol.,* **18**, 415-412 (2007).

[98] Brand U and Hillmann W, “Calibration of step height standards for nanometrology using interference microscopy and stylus profilometry.” *Precis. Eng.,* **17**, 22-33 (1995).

[99] Misumi I, Gonda S, Kurosava T and Takamasu K, “Uncertainty in pitch measurement of one-dimensional grating standards using a nanometrological atomic force microscope.” *Meas. Sci. Technol.,* **14**, 463-471 (2003).

[100] Misumi I, Gonda S, Kurosava T, Azuma Y, Fujimoto T, Kojima I, Sakurai T, Ohmi T and Takamasu K, "Reliability of parameters of associated base straight line in step height samples: Uncertainty evaluation in step height measurements using nanometrological AFM." *Precis. Eng.,* **30**, 13-22 (2006).

[101] Decker JE, Eves BJ, Pekelsky JR and Douglas RJ, "Evaluation of uncertainties in grating pitch measurement by optical diffraction using Monte Carlo methods." *Meas. Sci. Technol.,* **22**, 027001 (6pp) (2011).

[102] Meli F, Thalmann R and Blattner P, "High precision pitch calibration of gratings using laser diffractometer." *Pric. 1st Int. Conf. on Precision Engineering and nanotechnology (Bremen)* ed. P McKeown, **2**, 78-81 (1999).

[103] Pekelsky JR, Eves BJ, Nistico PR and Decker JE, "Imaging laser interferometer for traceable grating pitch calibration." *Meas. Sci. Technol.,* **18**, 375-383 (2007).

[104] Misumi I et al., "Submicrometre-pitch intercomparison between optical diffraction, scanning electron microscope and atomic force microscope." *Meas. Sci. Technol.,* **14**, 2065–74 (2003).

[105] Chen C-J, Pan S-P, Chang L-C and Peng G-S, "Pitch calibration by reflective laser diffraction." *Proc. SPIE* 5190, 156–64 (2003).

[106] Buhr E, Michaelis W, Diener A and Mirandé W, "Multi-wavelength VIS/UV optical diffractometer for high-accuracy calibration of nano-scale pitch standards." *Meas. Sci. Technol.,* **18**, 667-674 (2007).

[107] Song WY, Jung KY, O B-H, Park BC and Ko YU, "Precision laser diffractometry for grating period measurements." *J. Kor. Phys. Soc.,* **45**, 1510–6 (2004).

[108] Korotkov VI, Pulkin SA, Vitushkin AL and Vitushkin LF, "Laser interferometric diffractometry for measurements of diffraction grating spacing." *Appl. Opt.,* **35**, 4782–6 (1996).

[109] Eves BJ, Pekelsky JR and Decker JE, "Uncertainty evaluation of the NRC imaging diffractometer." *Meas. Sci. Technol.,* **19**, 075103 (2008).

[110] Meli F, Klein T, Buhr E, Frase CG, Gleber G, Krumrey M, Duta A, Duta S, Korpelainen V, Bellotti R, Picotto GB, Boyd RD and Cuenat A, "Traceable size determination of nanoparticles, a comparison among European metrology institutes." *Meas. Sci. Technol.,* **23**, 125005 (2012).

[111] Husu H, Saastamoinen H, Laukkanen T, Siitonen S, Turunen J and Lassila A, "Scatterometer for characterization of diffractive optical elements." *Meas. Sci. Technol.,* **25**, 044019 (2014).

[112] Hemming B, Korpelainen V, Seppä J and Lassila A, "Traceability for surface roughness measurement by metrology AFM." *Proc. of the euspen international conference San Sebastian,* June 2nd - 5th (2009), 243V2-246V2.

[113] Seppä J, Korpelainen V, Bergstrand S, Karlsson H, Lillepea L and Lassila A, "Intercomparison of lateral scales of scanning electron microscopes and atomic force microscopes in research institutes in Northern Europe." *Meas. Sci. Technol.*, **25**, 044013. (2014).